1-1-1998

Graded ferroelectric devices: the dielectric analogues of semiconductor diode junctions

Majed S. Mohammed

GRADED FERROELECTRIC DEVICES: THE DIELECTRIC ANALOGUES OF SEMICONDUCTOR DIODE JUNCTIONS

by

MAJED S. MOHAMMED

DISSERTATION

Submitted to the Graduate School

of Wayne State University,

Detroit, Michigan

in partial fulfillment of the requirements

for the degree of

DOCTOR OF PHILOSOPHY

1998

MAJOR: ELECTRICAL ENGINEERING
(Solid State Devices)

Approved by:

Gregg W. Chen 4/21/98
Advisor Date

Ratna Naik (Co. Advisor)

Joseph V. Mantese

Peter Lazaj

ACKNOWLEDGMENTS

I wish to express my deepest gratitude to my dissertation committee, Dr. Gregory Auner, Dr. Ratna Naik, Dr. Joseph Mantese and Dr. Pepe Siy, for their assistance and guidance in this research effort. This work would not have been possible without their selfless sharing of their time, knowledge and resources. My thanks are also extended to all members of the GFD project at General Motors Research and Development Center, Norman Schubring, Adolph Micheli, Andrew Mance and Antonio Catalan, for their valuable suggestions and much appreciated assistance.

I also wish to thank my family for their collective support and encouragement throughout the years. In particular, I would like to thank my father for believing in me and encouraging me all the way. I thank my mother for the boundless love and concern she never ceased to give, and finally I thank my wife, Dima, for her love, patience and support. To her I dedicate this work.

PREFACE

Ferroelectric materials have been used extensively for numerous applications, notably as capacitor materials for ultra large scale integration (ULSI) dynamic access memory (DRAM) for memory densities higher than 64 Mbyte and as sensing element in non-cryogenic infrared detection systems. In recent years, substantial research and development has been devoted to single crystals, polymers, composites and specially thin film ferroelectrics. However, most of these studies were confined to homogeneous ferroelectrics and very few have dealt with ferroelectric heterostructures. This work is a study of the microstructure and dielectric properties of barium strontium titanate thin films with gradient in composition normal to the growth surface. These ferroelectric heterostrcutures, referred to as graded ferroelectric devices (GFD's), share many similarities with semiconductor heterostructures. The GFD's can be considered as the dielectric (capacitive) analog of semiconductor trans-resistive (*transistor*) p-n or n-p diodes and to emphasis this equivalency a special term has been coined to describe these structures, trans-capacitors or *transpacitors*.

This thesis is divided into six chapters. Chapter 1 is an introduction to basic physics of ferroelectricity and a summary of the main properties of the barium strontium titanate ferroelectric system. Graded ferroelectric structures are discussed in chapter 2, with special emphasis on GFD's with compositional gradient. Chapter 3 is a study of the microstructure and dielectric properties of homogeneous BST films prepared by metallorganic decomposition (MOD). Analysis of the microstructure and dielectric properties of BST-GFD, as well as a phenomenological model that describes the unique properties of BST-GFD are given in chapter 4. A comparison of the effective and conventional pyroelectric coefficients obtained from graded and homogeneous BST is detailed in chapter 5. Finally, a discussion of the results and suggestions for future work are provided in chapter 6.

TABLE OF CONTENTS

LIST OF TABLES

LIST OF FIGURES

Chapter 6

Appendix A

Chapter 1

Introduction

1.1 : Basic Concepts and Definitions:

Crystals in nature can be classified into 32 crystal classes (point groups) according to their symmetry with respect to a point. A common feature among 11 of these point groups is the existence of a center of symmetry and are referred to as *centrosymmetric* materials. These crystals posses no polar properties. A uniform stress applied to a centrosymmetric crystal will result in a small and uniformly distributed displacement of the charges about the center of symmetry and the net polarization of the crystal will be zero. If, on the other hand, a uniform electrical field is applied to a centrosymmetric crystal, a uniform stress will be created within the crystal. The induced stress is proportional to the square of the applied field and a reversal in the field's polarity will not affect the sense of the induced stress. This phenomenon is known as *electrorestriction* and is common to all substances, crystalline or otherwise.[1]

With the single exception of the cubic class 432, all remaining 21 crystal classes have one or more polar axes. These crystals exhibit the phenomenon of *piezoelectricity*. When a piezoelectric crystal is subjected to a uniform mechanical stress, an electric field will be established inside the crystal. Unlike electrostriction, the piezoelectric effect and its converse, i. e. the production of strain by application of electric field, are linear. A reversal in the direction of the stimulus will lead to a reversal of the response. Piezoelectrics are equally divided into polar and non-polar crystals. Polar crystals have non-vanishing electrical dipole moment per unit volume (*spontaneous polarization*). The surface charge due to this built in dipole moment in general can not be detected directly since it is usually masked by the charge carriers that have reached the surface by internal or external conduction. An indirect method to measure the spontaneous polarization in polar crystals

makes use of the fact the magnitude of the spontaneous polarization is proportional to temperature, and by cooling or heating the crystal, charge will flow from or into the crystal and a current proportional to the change in temperature can be measured. The current due to the internal and external conduction is not large enough to compensate for the change in dipole moment[2]. As a result to their dependence on temperature, polar crystals are also known as *pyroelectrics*.

Ferroelectrics are a subgroup of pyroelectrics. Among pyroelectrics, the main feature that distinguish between ferroelectric crystals and non ferroelectric crystals is that in ferroelectrics the polarity of the spontaneous polarization can be reversed by an application of sufficiently high electric field. This gives rise to a non-linear dielectric hysteresis characteristic of ferroelectrics and similar to the hysteresis loops obtained in fereromagnetics. A typical plot of the net polarization versus applied field is shown in Fig. 1.1. The origin of hysteresis loops in ferroelectrics can be understood on the basis of the concept of *domains*.[3] Domains are regions of homogeneous polarization with negative and positive polarity. The terms positive and negative refer to spontaneous polarization being parallel or antiparallel to a specific crystallographic direction. Before the application of the electric field, the crystal has equal number of positive and negative domains. The overall polarization of the crystal is equal to zero and the depolarization field is minimum. A strong electric field parallel to the positive direction will switch all domains in the positive direction and the crystal is called a *single domain crystal* . Reducing the magnitude of the field will result in some of domains switching in the opposite direction. At zero field, the net polarization will have a non vanishing value as some of the domains still remain aligned in the positive direction. The finite polarization value at zero field is known as *remnant polarization* (P_r). If the linear portion is extrapolated back to the polarization axis, the intersection point represents the *spontaneous polarization* (P_s) value of the crystal. The *coercive field* (E_c) is defined as the field needed to reduce the polarization to zero. As the field is increased further in the negative direction, more and more positive domains will switch orientation and the crystal will become a single domain crystal with negative

polarity[3].

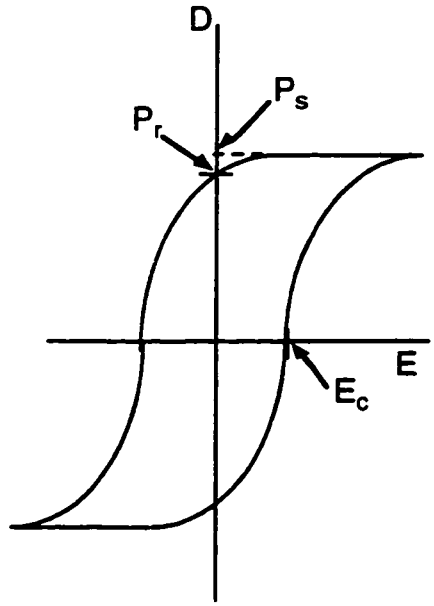

Fig. 1.1: A typical Ferroelectric P-E hysteresis loop

The area enclosed within the hysteresis loop represents the energy stored in the ferroelectric material and is equal to the energy needed to twice reverse the polarization. In a single domain ferroelectric, spontaneous polarization at zero applied field has only two possible values corresponding to the two opposite orientations allowed, while in a multi-domain ferroelectric the spontaneous polarization can take any value between these two extremes. In principle, a perfect crystal has equal remnant polarization (Pr) and spontaneous polarization values and the hysteresis loop would resemble a rectangle. However, in a less than perfect crystals (or samples) , the remnant polarization is different from the spontaneous polarization value and as a result of internal and external stresses reverse causing nucleation before applied field reversal, hence the free charge in the crystal can not reach their new equilibrium distribution during each half cycle.

Whereas the piezoelectricity and pyroelectricity of a crystal can be determined from x-ray spectroscopy, the ferroelectricity of a crystal can be only determined through dielectrical measurements. In other words, Ferroelectricity is a dielectric property of the crystal and not crystallographic property. The Sawyer-Tower hysteresis circuit is

commonly used to test ferroelectricity and measure the above ferroelectric quantities (P_r, P_s, E_c) in any sample. The circuit consists of a known linear capacitor C_o connected in series to with the sample C_x. The voltage across C_o is proportional to charge - and hence to the polarization - on the surface of the sample C_x. This voltage is connected to the vertical plates of the oscilloscope. The voltage on the horizontal plates is proportional to the voltage -and hence to the electric field- across C_x [4].

The spontaneous polarization and dielectric constant of ferroelectric crystals show strong dependence on temperature. The spontaneous polarization generally decreases with increasing temperature and becomes zero at a certain temperature T_c. This temperature also signifies a transition in the ferroelectric crystal from a polar phase to a non-polar phase. This transition temperature is often referred to as the *Curie point* in analogy with ferromagnetism. The low temperature phase is called the *ferroelectric phase* while the high temperature phase is called *paraelectric* (or non-polar) phase.

The *dielectric displacement* (D) of any material is related to the spontaneous polarization and the applied field through the relation:

$$D = \varepsilon E + P_s \qquad (1.1)$$

where ε is the *dielectric constant* of the material and is normally defined as the derivative of the dielectric displacement vector D with respect to the field E. For a normal or linear dilelectric material ε is a constant independent of applied fiield but in the case of ferroelectrics, due the compilcated dependency of the dielectric displacemnt on electric field (hysteresis), the dielectric "constant" is in reality a function of applied field and is usually defined as the slope of the D-E curve at the origin $\varepsilon = \left(\frac{\partial D}{\partial E}\right)_{E=0}$ It is customary to measure this initial dielectric constant with a very small a.c. field in order to avoid reversing any domains. [3]

Single crystal ferroelectrics show a very high peak in ε at Curie point. Above the transition temperature, the dielectric constant follows the well known Curie-Weiss law

$$\varepsilon = \varepsilon_o + \frac{C}{T-\theta} \qquad (1.2)$$

where the ε_o is the temperature independent electronic contribution, C is the *Curie Constant*, T is the absolute temperature and θ is the *characteristic temperature*. The characteristic temperature θ is identical to the Curie transition temperature T_c only in the case of second order (continuous) transition from the polar ferroelectric phase to the non-polar paraelectric phase and for a first order (abrupt) transition the value of θ is usually lower than T_c.

An interesting phenomenon that is closely related to ferroelectricity is *antiferroelectricty*. Like ferroelectrics, with decreasing temperatures, antiferroelectrics show a transition from a crystal phase with higher symmetry to a phase with lower symmetry. Similarly, a high dielectric constant peak is observed at the transition temperature and above this temperature the dielectric constant follows the Curie-Weiss relation. However, in contrast to ferroelectrics, the lower symmetry phase is non-polar and as a result, the net polarization of the crystal is zero. The contrast in dielectrical behavior between ferroelectrics and antiferroelctrics can be traced back to the difference in dipole moment configuration between these two structures. In ferroelectrics the point dipoles are all parallel and point in the same direction while in antiferroelectrics the point dipoles are anti-parallel to each other as shown in Fig.1.2. What determines why a certain structure is a ferrolectric while another is a antiferroelectric is the condition of minimum free energy. For the hypothetical simple cubic structure shown in Fig 1.2 free energy calculations show that configuration A [anti-parallel = anti-ferrolectric] has lower free energy than that of configuration P [parallel = ferroelectric], or in other words the anti-ferrolectric configuration is the stable state and the ferroelctric configuration would be a metastable state only. The example, a simple cubic is an oversimplification and in more complicated structures the ferrolectric configuration is the stable state. Antiferroelectric configurations,

however, do occur in lattices which are more complicated than the simple cubic and the most notable examples of naturally existant antiferrolelectrics are ammonium dihydrogen phosphate ($NH_4H_2PO_4$), sodium niobate ($NaNbO_3$) and lead zirconate ($PbZrO_3$). Like ferroelectricity, antiferroelectricity is not a crystallographic property and can only be established through dielectric measurements.[1]

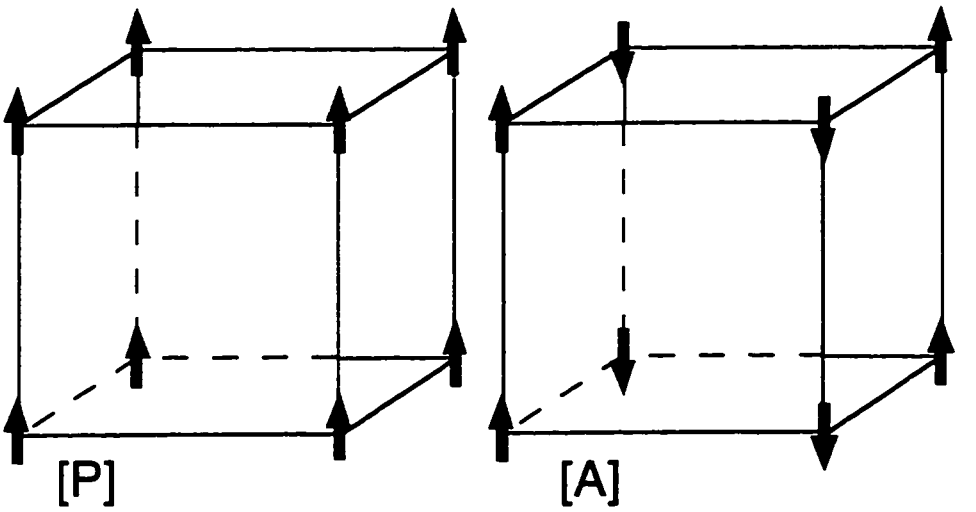

Fig. 1.2: Anti-parallel (A) and Parallel (P) dipole arrangements in simple cubic structure

1.2 : Ferroelectric Properties of Barium Titanate

The ferroelectricity of barium titanate ($BaTiO_3$) was first reported by Von-Heppel [5] (1945) and Wul and Goldman[6] (1946). The discovery came nearly a quarter a century after the discovery by Vlasek[7] (1920) of ferroelectricity in Rochelle salt, which is considered the first ferrolectric material and was preceded by an independent discovery in 1943 of the anomalous dielectric properties of ceramic $BaTiO_3$ by Wainer and Salomon (USA), Ogawa (Japan) and Wul and Goldman (Russia). The first single crystal $BaTiO_3$ was produced in Switzerland in 1947, however, the method for growing large single crystals with excellent crystal and ferroelectric properties was not perfected till 1954 with the invention of the Remeika method[8]. In this technique a mixture is prepared from 30% $BaTiO_3$ and 70%

potassium fluoride which functions as a flux. Small amounts of Fe_2O_3 is added to the mixture in order to reduce the conductivity of the crystals which arises from the loss of oxygen at high temperatures. The mixture is placed in a platinum crucible and heated in a furnace at temperatures in the 1150-1200°C for 8 hours. The crucible is then cooled slowly to about 800-850°C. At this temperature the liquid flux is poured off and the crystals are further cooled down to room temperature. This technique produces larger crystal plates of triangular shapes with hypotenuses which are as long as 2-3 cm and thickness of few millimeters.

The discovery of ferrolectricity in $BaTiO_3$ renewed the interest in ferroelectrics. The crystal structure of $BaTiO_3$ is far simpler than any other ferroelectric crystal known to date. $BaTiO_3$ is also easier to study and offers greater potential for practical application due to its chemical and mechanical stability. $BaTiO_3$ is ferroelectric at and above room temperature, and can be easily prepared and used in the form of ceramic and thin film polycrystalline samples.

Barium titanate belongs to a group of ferrroelectrics known as *perovskite-type* ferroelectrics. These structures are named after the mineral CaO_3 also known as perovskite. Perovskite-type ferroelectrics are subgroup of a larger group of ferroelectrics known as *oxygen-octahedra* ferroelectrics. A cubic pervoskite unit cell in $BaTiO_3$ is shown in Fig. 1.3. The common chemical formula for pervoskite-type ferroelectrics is ABO_3, where the cations A are located at the corners of the cube, cation B is at its center and the oxygen anions are face centered.

The tolerance factor for $BaTiO_3$ can be easily calculated form:

$$t = \frac{R_{Ba} + R_O}{\sqrt{2}(R_{Ti} + R_O)}$$

where R_{Ba}, R_{Ti} and R_O are the ionic radii of Ba, Ti and O respectively. Substitution $R_{Ba} = 1.43\text{Å}$, $R_{Ti} = 0.64$ and $R_O = 1.32$ give $t = 1.02$. A tolerance factor value of 1 indicates that packing in the crystal is ideal, and a tolerance factor value greater than 1 (as is the case for $BaTiO_3$) indicates that the Ti cation has more space around it and hence it can

"rattle" freely inside the octahedron. This result is of great value to the understanding of the origin of ferroelectricity as will be discussed in the section devoted to Slater's model (section 1.4).

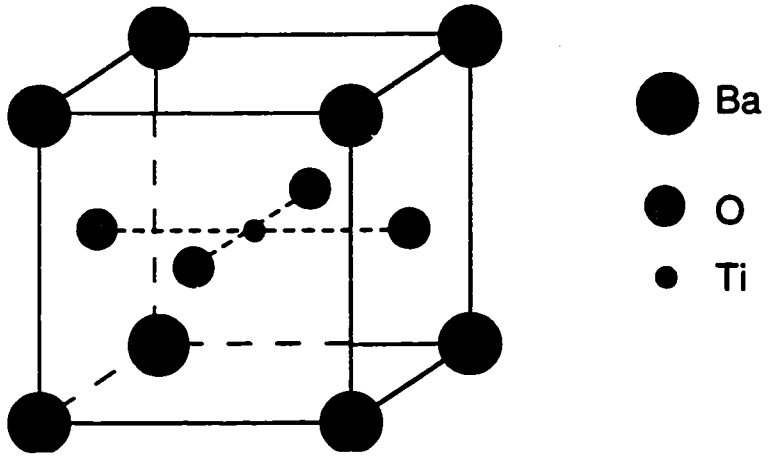

Fig. 1.3: The cubic perovskite-type structure in $BaTiO_3$

The curie temperature of single crystal $BaTiO_3$ is 120 °C. Above this transition temperature, $BaTiO_3$ has cubic (point group m 3 m) non polar phase, and the phase below this transition temperature is ferroelectric tetragonal (point group 4 m m). In the ferroelectric phase the spontaneous polarization is along the tetragonal c axis. The tetragonal structure results when one of the cubic original edges is elongated along the <100> direction forming the c axis, and the other two axes are compressed to form the a axes. At room temperature the ratio of c/a is about 1.01.

Between 5 °C and -80 °C $BaTiO_3$ has orthorhombic structure (point group m m). The orientation of the spontaneous polarization is along the <110> direction (face diagonal) of the original cubic phase. Below -80°C the crystal phase is rhombohedral (point group 3m) and the polar axis is directed along the <111> (body diagonal) direction of the paraelectric cubic phase. As typical for all ferroelctrics, the above phase transitions are accompanied by notable changes in the values of the dielectric constant and spontaneous polarization[9].

The temperature dependence of the dielectric constant for single crystal $BaTiO_3$ is shown in Fig 1.4. Above the transition temperature the crystal has a cubic structure and the dielectric constant follows the Curie-Weiss law. The Curie constant is a measure of the temperature dependence of the dielectric constant. Based on their Curie constant values, ferroelectrics can be classified into two groups. In the first group, the dipoles are all parallel and are oriented in either of the two opposite directions corresponding to the two equilibrium orientations. The Curie constant in this case in the order of 3θ where θ is characteristic temperature (~300K) and thus C is in the order of 10^3. In a ferroelectric material belonging to the second group an electric dipole moment is produced when the ions present in the material are displaced from their equilibrium positions. The temperature dependence of the dielectric constant for the ferroelectrics in the second group is small and hence the Curie constant is large and is typically of the order of 10^5. Among the better known ferroelectrics, Rochelle salt and Tri-glycine sulfate belong to the first group while barium titanate and potassium niobate belong to the second group. For BaTiO3, the Curie constant strongly depends on the purity of the specimen, and different values for the Curie constant of single crystal $BaTiO_3$ are quoted in literature but are generally in the range of 1.5 to 6.5 $x10^5$ degrees. Since the spontaneous polarization transitions in $BaTiO_3$ single crystals are of the first order* it is expected that the characteristic temperature θ will differ slightly from the Curie transition temperature T_c. Best estimates of θ are obtained for polycrystalline $BaTiO_3$ and is about 118°C compared to 130°C for T_c. A maximum value for the dielectric constant exists at the Curie point and is close to 10,000. Few other ferroelectric material exhibits such a high value for the dielectric constant. Below the transition temperature it is clear from Fig 1.4 that there are two branches in the dielectric

---

* A first order transition is characterized by a sudden "jump" in the spontaneous polarization at $T=T_c$ from $P_s=0$ above T_c to $P_s=Po$ below T_c, where P_o is the spontaneous polarization value in the ferroelectric phase. On the other hand, in a second order transition the transition from $P_s=0$ to $P_s=P_o$ is continuous.

constant curve corresponding to measurements along the c and a axes. In general, ε_a is significantly larger than ε_c and at room temperature the values for ε_a and ε_c are approximately 200 and 4000, respectively. A 10°C thermal hysteresis is observed in the dielectric constant curves about the transition temperatures corresponding to transitions from tetragonal to orthorhombic and from orthorhombic to rhombohedral. A smaller hysteresis - not apparent in Fig. 1.4- exists for the transition from the cubic phase to the tetragonal phase. The existence of thermal hysteresis can be traced back to the fact that all of the above transition are of the first order type[3].

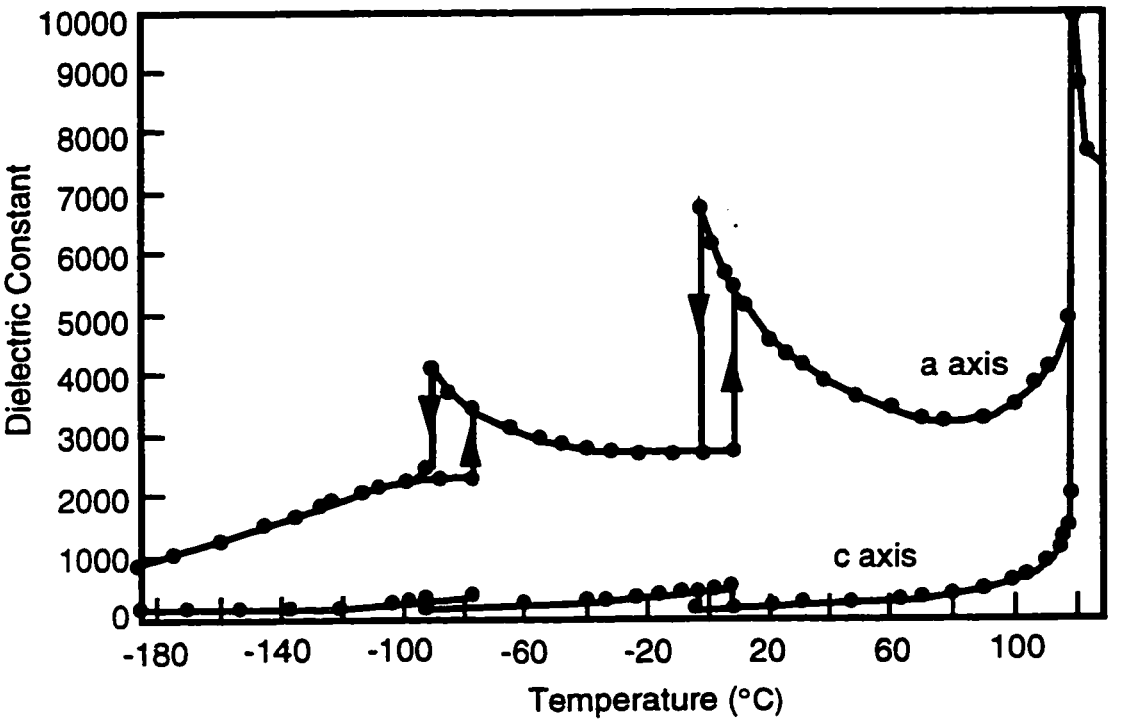

Fig. 1.4: The dielectric constant of $BaTiO_3$ as a function of temperature.

The temperature dependence of the spontaneous polarization of $BaTiO_3$ is shown in Fig. 1.5a. Although the transition at Curie point from the ferroelectric state to the paraelectric state appears to be of the second order (continuous), careful examination of the transition using high quality crystals shows that the transition is of the first order (discontinuous) as shown in Fig. 1.5b. At room temperature, the value of the spontaneous polarization for $BaTiO_3$ single crystals is 26 $\mu C/cm^2$. The P_s value is significantly lower

for ceramic and thin film samples.

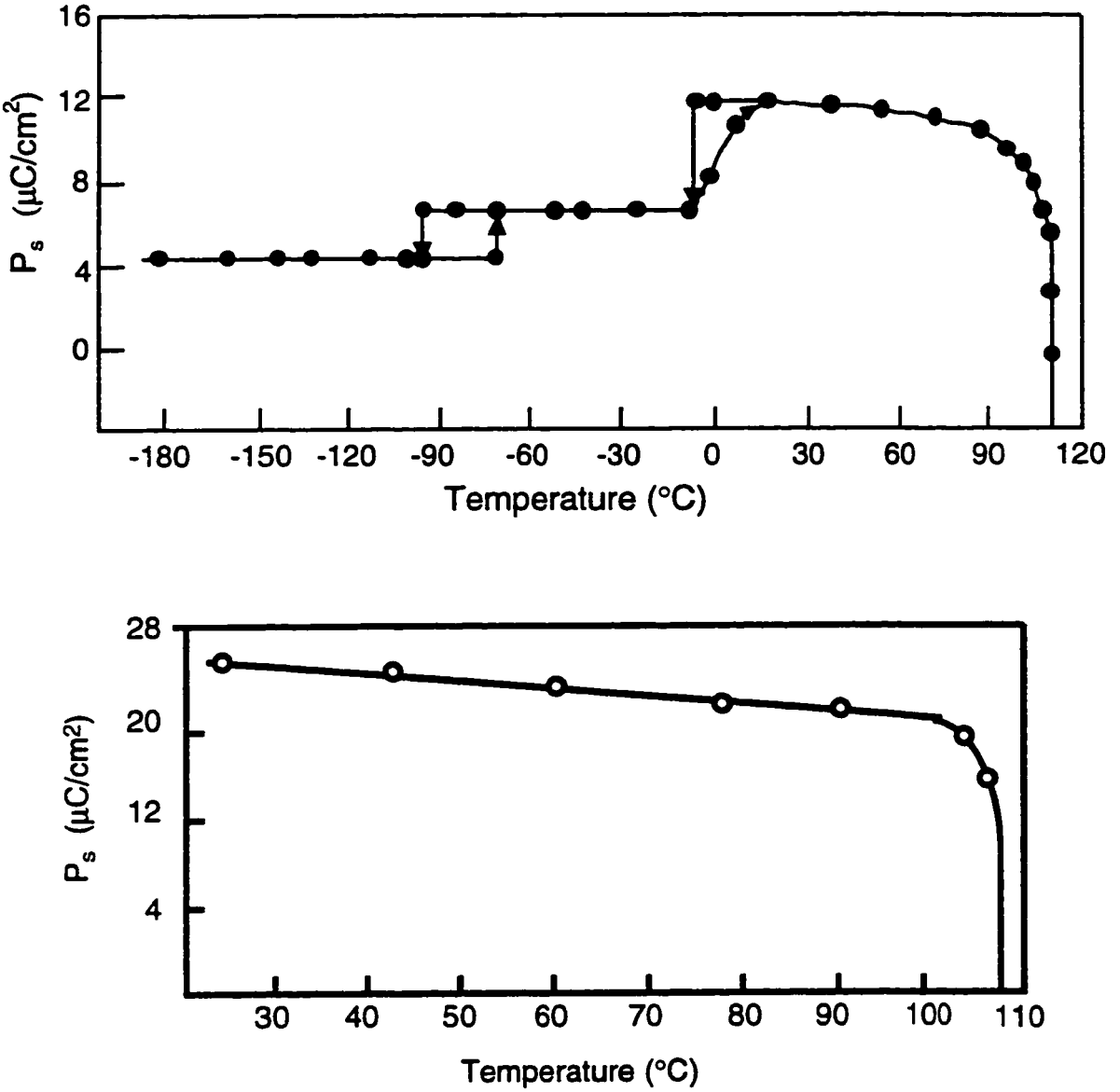

Fig. 1.5: (a) Temperature dependence of the spontaneous polarization of $BaTiO_3$, (b) The first order transition in spontaneous polarization at Curie point.

1.3: The $Ba_xSr_{1-x}TiO_3$ System

Strontium titanate ($SrTiO_3$) has a perovskite-type structure similar to barium titanate. However, unlike barium titanate there is a great deal of uncertainty regarding the ferroelectricity of strontium titanate. Smolinsky[10,11] observed a peak in the dielectric constant of ceramic $SrTiO_3$ around 20-30 K. The value of the dielectric constant at the peak

is 2000 and at room temperature is about 300. At high temperatures the dielectric constant of $SrTiO_3$ follows the Curie-Weiss law and an extrapolation of this relation suggests a ferroelectric transition at about 30-40 K. On the other hand, other studies[12] reported that no peak in the dielectric constant was ever observed even at temperatures as low as 4 K and thus concluded that $SrTiO_3$ is not a ferroelectric. However, more recent studies reported that a transition from a paraelectric state to a ferroelectric do occur in $SrTiO_3$ and the transition temperature is in the range of 4.2[13] - 75[14] K depending - among other factors - on the quality of the specimen and the accuracy of the measurement technique.

Application wise, there are very few products that employ pure $SrTiO_3$ or pure $BaTiO_3$. $SrTiO_3$ has low dielectric constant at room temperature and an extremely low transition temperature (if it exists). $BaTiO_3$, on the other hand, has an impressive dielectric constant peak value at the transition temperature, However, this transition temperature (T_c=120 °C) is too high for most applications where a high dielectric constant is desirable.

A different situation exists for the solid solution $Ba_xSr_{1-x}TiO_3$. Addition of Sr to $BaTiO_3$ lowers the transition temperature of $BaTiO_3$, as shown in Fig. 1.6a. The ferroelctric transition in the compound $Ba_{0.7}Sr_{0.3}TiO_3$ takes place near room temperature. It is interesting to note that the decrease in transition temperature of $BaTiO_3$ due to the addition of $SrTiO_3$ does not decrease the dielectric constant value but to the contrary the $Ba_xSr_{1-x}TiO_3$ solid solutions have higher peak values than pure $BaTiO_3$[14]. The above properties of the $Ba_xSr_{1-x}TiO_3$ system makes it very useful for a wide range of applications. Such applications include dynamic random access memories (DRAM), thermistors, infrared detectors, and phase array antennas. In this study, a new item is added to the above list of $Ba_xSr_{1-x}TiO_3$ applications, namely in the formation of graded ferroelectric devices (GFD's).

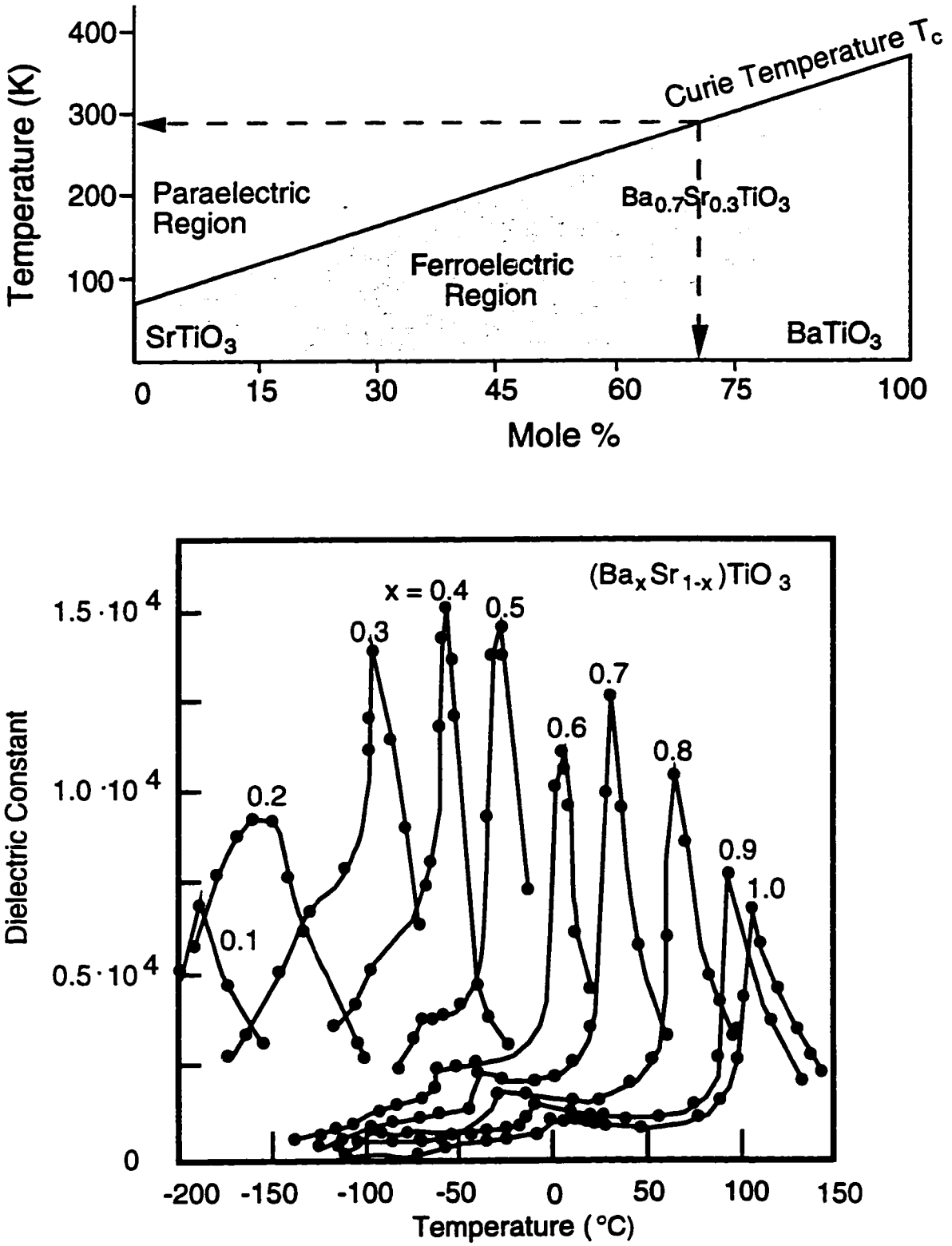

Fig. 1.6: (a) The transition temperature in $Ba_xSr_{1-x}TiO_3$ as a function of Sr concentration, (b) The dielectric constant of $Ba_xSr_{1-x}TiO_3$ as a function of temperature.

1.4 : Slater's Phenomenological Model for $BaTiO_3$

Over the years, many theories and models were suggested to explain the origin of ferroelectricity in $BaTiO_3$ and other ferroelectrics. The most successful of these models are the theories of Devonshire[16-18] and Slater[19]. In the following a brief description of the basic ideas of each model will be given. However, the Slater model will be discussed in slightly more detail since it forms the basis of the model proposed in this study for graded ferroelectric devices.

In the Devonshire model, the free energy $\mathcal{E}$ is expressed in terms of increasing powers of polarization

$$\mathcal{E} = \frac{1}{2}\chi^s\left(P_x^2 + P_y^2 + P_z^2\right) + \frac{1}{4}\xi_{11}^s\left(P_x^4 + P_y^4 + P_z^4\right) + \frac{1}{2}\xi_{12}^s\left(P_x^2P_z^2 + P_y^2P_x^2 + P_z^2P_y^2\right) + \ldots \quad (1.4)$$

where P_x, P_y, and P_z represent the component of polarization along the x, y, and axes. χ^s, ξ_{11}^s, ξ_{12}^s are temperature dependent expansion coefficients. The superscript s indicates that these quantities are measured at constant stress. Only even powers of P are included in the expression for free energy since it is assumed that the free energy remains unchanged when the polarization reverse signs. By successive differentiation of the free energy with respect to P and substituting the known values of the Curie transition temperature T_c, characteristic temperature θ, Curie constant C, and the spontaneous polarization P_s value at one temperature in the tetragonal phase, this model is capable of explaining most of the characteristic properties of ferroelectrics. Most notably, the Devonshire model was successful in predicting the temperature dependence of the dielectric constant, spontaneous polarization, and spontaneous strain. The predicted dependence of the dielectric constant on temperature is shown in Fig. 1.7.

Slater's model is based on the assumption that the free energy of a perovskite-type ferroelectric system can be written as[20]:

$$\mathcal{E} = k_o(T - T_c)x^2 + Bx^4 \qquad (1.5)$$

where x is the ion displacement relative to the central charge, T the absolute temperature, T_c Curie transition temperature and k_o and B are characteristic functions of the ferroelectric material.

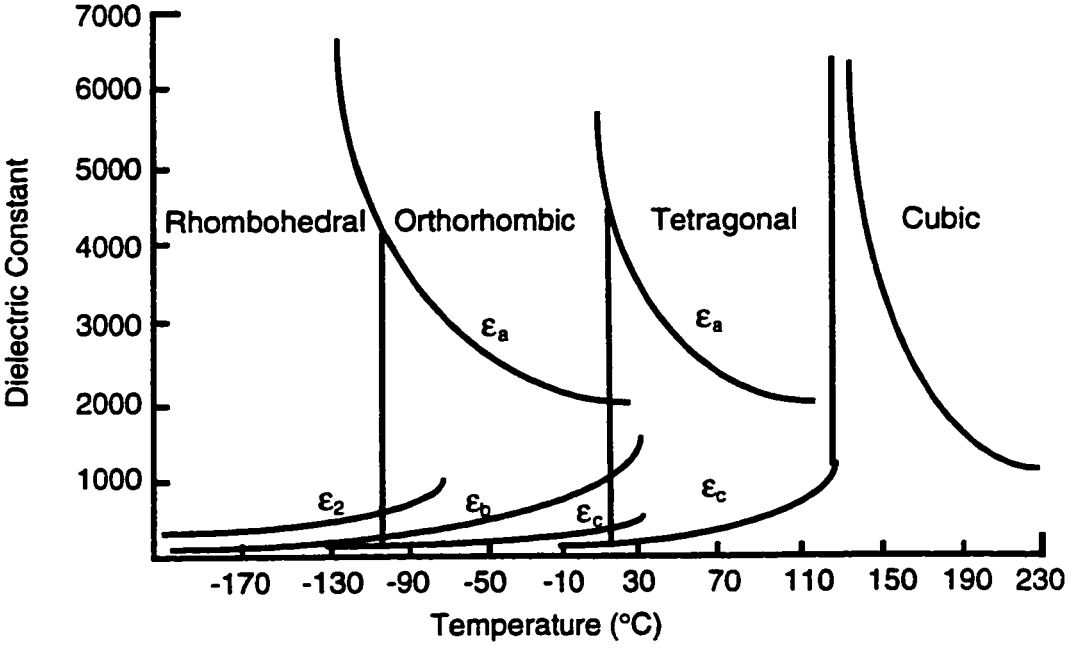

Fig. 1.7: Dependence of the dielectric constant of $BaTiO_3$ on temperature (Devonshire model).

Fig. 1.8 is a plot of the free energy as a function of displacement at different temperatures. Below the transition temperature, $\mathcal{E}$ has two minima at $x = \pm\sqrt{\frac{k_o(T_c - T)}{2B}}$ and a maximum between at $x = 0$. The maximum symbolizes the unpolarized state of the system (unstable equilibrium position) and the two minima symbolize the two polarized states characteristic of the perovskite structure. As the temperature is increased, the two minima approach each other to form a single minimum at $T=T_c$. Consequently, the polarization of the ferroelectric system being the product of the displacement of the ions times the charge carried by the ion vanishes at $T=T_c$.

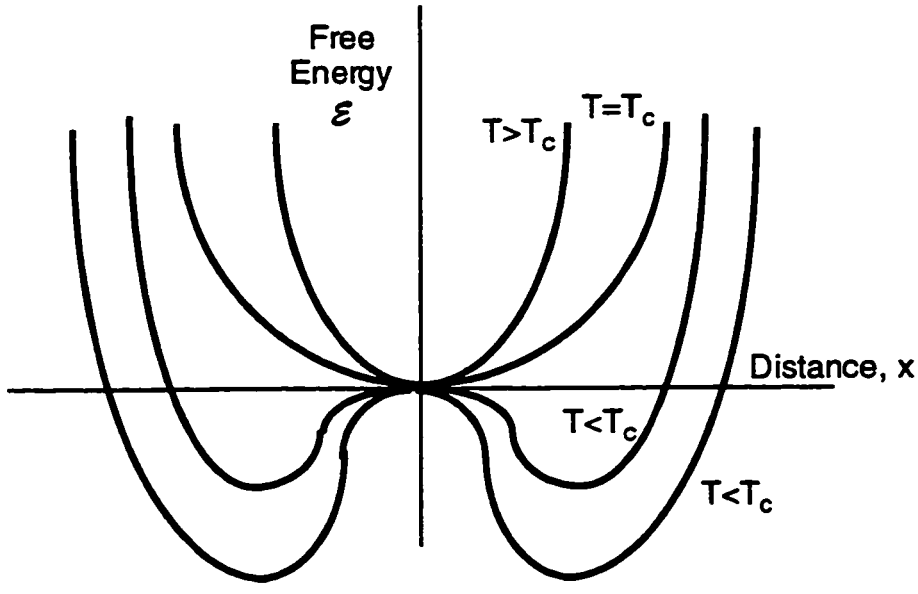

Fig. 1.8: The free energy $\mathcal{E}$ as a function of temperature according to Slater's model

The origin of the D-E hysteresis in ferroelectrics can be easily explained with Slater's model. The energy due to an external electric field is represented by an additional term to the free energy expression given by eq. 4.

$$\mathcal{E} = k_o(T - T_c)x^2 + Bx^4 - Ax \qquad (1.5)$$

Where A is a constant proportional to the field. Below the transition temperature, the ferroelectric system is in one of two minima sites, say the left hand minimum. Application of the electric field lowers the right hand minimum and raises the left hand minimum. Increasing the electric field, this process continues until some critical field value ($E = E_1$), where the left hand minimum will be at a level above the maximum at the origin. At this point the left hand minimum is not an equilibrium site anymore and the point representing the system will slide over to the much deepend right hand minimum. This will result in a reversal of the polarization of the system. The situation is reversed when the electric field switches polarity and at a second critical field value that is equal in magnitude but opposite in sign to E_1 there will be another reversal in polarization back to the original state.

Finally, Slater's model is capable of explaining the observed anomaly in the dielectric constant. The dielectric constant is inversely proportional to the elastic constant k which is in turn proportional to the curvature of the energy parabola. At temperatures above the transition temperature the free energy curve will have a minimum at the origin and by increasing the temperature of the system, the curvature of the energy curve increases and as a result the dielectric constant will decrease. Below the transition temperature the system is in equilibrium at any of the two minima. Cooling the system to temperatures below the transition temperature will result in an increase in the curvature of these minima and the dielectric constant will decrease again. The dielectric constant is theoretically infinite at $T=T_c$.

According to Slater's model, the physical mechanism responsible for the temperature dependence of the elastic constant k and consequently the temperature dependence of the free energy is Lorentz correction[20]. If an external electric field E is applied to a crystal with cubic symmetry then the local field at the position of an ion in the crystal is not equal to the average field but is given by $E_{loc} = E + \frac{4\pi}{3}P$, where P is the ionic polarization and is equal to Nex where N is the number of ions per unit volume. Taking the Lorentz correction into consideration, the effective square of the resonant frequency of the system ω_o^2 is changed to $\omega_o^2 - (4\pi/3)(Ne^2/m)$. The resonant frequency is proportional to the elastic constant and is a product of the short range forces that arises from the attractions and repulsions between neighboring ions. In-depth analysis of the terms involved in the new form for the resonant frequency reveals that in this expression ω_o^2 has similar temperature dependency as the elastic constant k given in eq. 1.4 and that the two terms in this expression cancel each other at $T=T_c$. The above conclusions form the physical basis of the Slater model.

Chapter 2

Graded Ferroelectric devices: Literature Survey

2.1: Introduction

As has been mentioned in the outline, the objective of this work is to study the microstructure and electrical properties of BST thin films with gradient in polarization due to gradient in composition across the films. In this chapter previous studies on ferroelctric materials with polarization gradient are reviewed. Homogeneous ferroelectric films are characterized by the existence of a built in spontaneous polarization that would switch polarity under sufficiently strong electric field. In polycrystalline films the spontaneous polarization is uniform across film thickness and has value that is significantly lower than that in ceramics and single crystals. Mantese et al[1] have shown that gradient in polarization normal to the growth surface is readily formed in ferroelectric materials when the polarization vector is coupled to gradients in temperature (∇T), strain ($\nabla \delta$), or composition (∇c). These structures are referred to as graded ferroelectric devices, or GFD's. Graded ferroelectric devices are a novel class of ferroelectrics that exhibit unique properties unseen in homogeneous ferroelectric single crystals or thin films.

Figure 2.1 show the spontaneous polarization of a typical graded ferroelectric thin film as a function of temperature T and normal distance z from the substrate. The choice of the reference point $z = 0$ is arbitrary. It is clear that at fixed z values the spontaneous polarization dependence on temperature is similar to that observed in homogeneous ferroelectric films. The spontaneous polarization is constant below a certain transition temperature $T_c(z)$ and is zero above $T_c(z)$. With increasing distance, the Curie transition temperature $T_c(z)$ increases and $P_s(z)$ at $T=T_c(z)$ decreases. This non-uniformity in

spontaneous polarization across the film give rise to the free energy diagram as shown in Fig. 2.2. With increasing z, the level of the originally horizontal potential wells is shifted in the manner shown in Fig. 2.2 as each of the individual wells is skewed towards lower energies. Application of alternating potential populates the lower energy wells resulting in a self poling effect that can be detected as measurable spontaneous potential across the graded ferroelectric device when the excitation is removed.

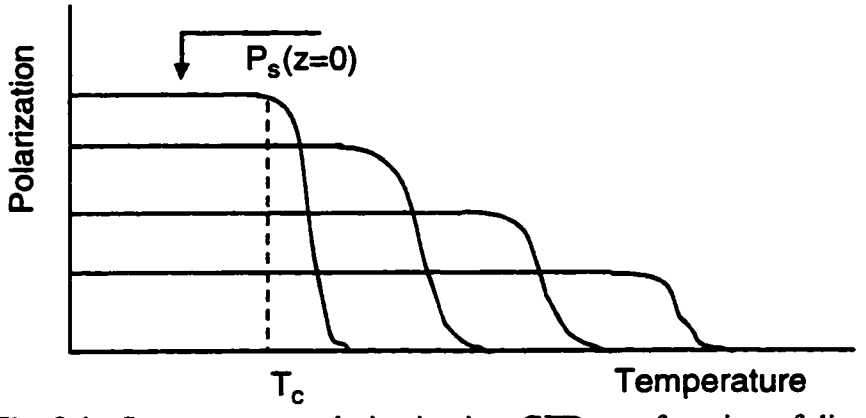

Fig. 2.1: Spontaneous polarization in a GFD as a function of distance

Fig. 2.2: Free energy of GFD's as a function of distance

The shift in the potential wells can be easily explained[1] by assuming that the spontaneous polarization in the sample has the form $P(z) = P_o + z\nabla P$. Assuming that the polarization due to the polarization gradient is small compared to P_o, i.e. $|P_o| << |z\nabla P|$,

substituting P(z) into Devonshire's free energy $\mathcal{E}$ (eq. 1.1), the shift in the free energy (i.e. built in potential) $\Delta\mathcal{E} = \mathcal{E}(P(z)) - (P_o)$ is simply expressed as $\Delta\mathcal{E} = Bz\nabla P$, where B is a function of temperature and is independent of z[+]. The concept of built in potential is very common in solid state physics. The complex behavior of semiconductor heterostructures such as diodes and transistors can be easily explained in terms of built in potential in the junction region(s).

2.2: Ferroelectric Structures Under Temperature Gradient

A homogenous ferroelectric is readily transformed into a graded ferroelctric when a temperature gradient ∇T is set up across the ferroelctric material. The temperature gradient creates a gradient in the strain as a result to the thermal expansion of the material. This strain gradient in turn give rise to a gradient in polarization ∇P across the sample[2,3]. Sukarov et al[4,5] studied the effects of variable temperature gradient (and hence variable ∇P) on the dielectric properties of Triglycine sulfate (TGS) single crystal.. Their results show that the temperature dependence of the spontaneous polarization and dielectric permittivity is not only a function of the magnitude of the temperature difference across the material but also depends on the relative orientation of ∇T with respect to the polar axis. The results were found to vary depending on whether the Curie temperature T_c of the ferrolectric material lies within or outside the applied temperature gradient. In the presence of temperature gradient, the effective dielectric permittivity can be written as:

$$\varepsilon = (T_2 - T_1)\left(\int_{T_1}^{T_2}[\varepsilon(T)]^{-1}dT\right)^{-1} \qquad \text{for } P_s \| \frac{dT}{dz}\mathbf{n}$$

$$\varepsilon = (T_2 - T_1)^{-1}\int_{T_1}^{T_2}\varepsilon(T)dT \qquad \text{for } P_s \perp \frac{dT}{dz}\mathbf{n} \qquad (2.1)$$

[+] For $|P_o| >> |z\nabla P|$ the built in potential is given as $\Delta\mathcal{E} = \bar{B}(z\nabla P)^2$ where $\bar{B}$ is independent of z.

where **n** is a unit vector in the direction of the spontaneous polarization, T_2 and T_1 are the lower and upper limits of the applied temperature difference. The effective polarization is defined as:

$$P^* = v^{-1}\int_v P_s dv \qquad (2.2)$$

where P_s is the spontaneous polarization of homogeneous ferroelectrics and v is the crystal volume:

$$P_s^2 = \frac{\alpha}{\beta}(T - T_c) \qquad (2.3)$$

where α and β are constants. In the special case when T1 <Tc <T2, the above expression for the effective polarization is reduced to :

$$P^* = \frac{2}{3}\frac{(\alpha/\beta)^{1/2}}{(T_2 - T_1)}(T_c - T_1)^{3/2} \qquad (2.4)$$

Comparison of the calculated permittivity and spontaneous polarization with the experimentally obtained data show an excellent agreement between the observed and calculated temperature dependencies of the permittivity when the temperature gradient is parallel to the polar axis. On the other hand, the calculated curves and the observed curves differ significantly when the direction of the temperature gradient is normal to the direction of the spontaneous polarization. With increasing temperature gradient, the calculated permittivity curves are smeared and the maximum permittivity value is shifted towards higher temperatures. A comparison between the calculated spontaneous polarization and the observed polarization reveal that at low temperature gradient values the curves are nearly identical regardless of the relative orientation of P_s and ∇T. At higher temperature gradients, the experimental P_s curves are displaced more towards low temperature values.

In the case when the Curie temperature lies outside the applied temperature range ($T_2 > T_1 > T_c$), a spontaneous polarization proportional to the temperature gradient is created in the paraelectric regime. The induced polarization has a maximum value at T_c and

decreases nonlinearly at lower temperature and linearly at higher temperatures. An induced potential difference (and hence an induced electric field) is created across the sample as a result of the induced polarization. This electric field is known *as "thermally generated electric field"* or TGEF. Sajosch[6] suggested that the induced potential in a single crystal can be written as

$$\phi = \frac{p}{\varepsilon\varepsilon_o}\nabla T \qquad (2.5)$$

where p is the pyroelectric coefficient of the ferroelectric material, ε and ε_o are the vacuum and crystal dielectric permittivities, respectively. In a simple model of a monoaxial ferroelectric of thickness d and surface area S $\left[d << (S)^{1/2}\right]$ and assuming short circuit boundary conditions, $\phi(z=0) = \phi(z=d) = 0$, then:

$$\phi = \frac{p}{2\varepsilon\varepsilon_o}\left(z^2 - zd\right)\nabla T \qquad (2.6)$$

and the induced electric field as a function of normal distance is:

$$E = \frac{p}{2\varepsilon\varepsilon_o}(d - 2z)\nabla T \qquad (2.7)$$

It can be clearly seen from the above argument that a uniform temperature gradient give rise to a non-uniform electric field in the sample. The induced TGEF is proportional to the pyroelectric coefficient and inversely proportional to the dielectric constant.

2.3: Ferroelectric Structures with Compositional Gradient

Unlike semiconductor heterostructures, there are comparably fewer studies on ferroelectric heterostructures available in literature. The majority of these studies are theoretical treatments of ferroelectric heterostructures based on the Landau-Ginzburg theory[7-10]. It was not until the advancement of new techniques for deposition of high quality metal-oxide thin films that more attempts to form ferroelectric heterostructures and study their microstructure and dielectric properties were reported[11-13]. Of particular interest

to the present study are thin ferroelectric films with compositional gradient normal to growth surface[1,14]. A gradient in polarization ∇P is readily formed in ferroelectrics with gradient in composition ∇c normal to the growth surface. The link between the composition gradient and the resulting polarization gradient can be easily explained in a manner similar to that of the induced polarization due to temperature gradient. The conjugation of adjacent layers with different composition (c) and different lattice parameter (a) create inhomegenoues intrinsic strain which in turn creates an inhomogenous polarization in the ferroelectric material. In an alloy with composition gradient along the z direction, the strain tensor is changing along the z-direction and the induced polarization can be written as:

$$\nabla P_s(z) = \gamma_{zz}\left(\frac{\Delta a}{a}\right)\left(\frac{dc(z)}{dz}\right) \qquad (2.8)$$

where γ_{zz} is an elasto-concentration coefficient. The above expression can be easily incorporated into the expression for total spontaneous polarization which can be rewritten as:

$$P_s(z) = P_s(c_o)\left(1+\frac{z}{c_o}\nabla c\right) \qquad (2.9)$$

where $P_s(c_o)$ is a constant independent of temperature and distance.

In general, ferroelectrics with compositional gradient exhibit similar dielectric permittivity and spontaneous polarization dependency on temperature as ferroelectrics with temperature or strain gradients. Schubring et al[14], in a recent study on potassium tantalate niobate (KTN) thin films with gradient in composition, have also reported a smearing in the dielectric permittivity curves and a shift in the maximum permittivity value towards higher temperatures. Similarly, hysteresis (i.e. spontaneous polarization) was found to persist well above the nominal Curie temperature. However, the most striking result of this study is a new phenomenon that had never been reported before for either homogeneous ferroelectrics or ferroelectrics with temperature or strain gradients. A better understanding

of this new phenomenon is the basis and major motivation behind the present study, and therefore it will be discussed with greater detail in the following.

The KTN films were formed on platinum coated polycrystalline yttria by metallorganic decomposition (MOD). Thin circular Au/Cr electrodes (area = 0.012 cm^2, thickness = 340 nm) were deposited on top of the KTN films by e-beam evaporation. Selective etching was used to electrically access the platinum layer which served as counter electrode. An unconventional hysteresis phenomenon was observed in the 9.8 μm thick films when excited by a strong electrical field. The observed hysteresis loops did not close upon themselves and developed a large offset along the dielectric displacement vector axis. The hysteresis offset is also observed as charge stored ($\nabla Q = \nabla D \cdot A$) across the serially connected integrating capacitor in the modified Sawyer-Tower circuit used in this experiment.

The origin of the hysteresis offset can be traced to the gradient in potassium concentration in the films. As part of the film growth process, the KTN films were annealed at 1100°C in the presence of excess potassium vapor supplied by potassium aluminate powder. X-ray depth profiling reveals that a gradient in potassium concentration normal to the growth surface exist in these films. This concentration gradient in turn give rise to a gradient in the $KNbO_3/KTaO_3$ ratio across the top layer of the film (2μm).

Elaborate set of tests were conducted to rule out any possible cause other than the concentration gradient as the origin of the charge offset[1]. No charge offset was observed in homogeneous KTN or BST films while uniaxial charge flow was observed in graded BST. This rules out space charge effects as the origin of this phenomenon. The fact that BST films contain no volatile components further strength the above conclusion. The asymmetry in contacts was ruled out as a cause for the charge offset in an experiment where the yttria substrate and the platinum overcoat were removed by selective etching and Au/Cr contacts were deposited on the film surface previously joined to the platinum layer thus creating a symmetric contact configuration. The direction of the charge offset relative

to the contacts was found to reverse. In another set of experiments, measurements were repeated using other metals such as In, Cr, Cu, and Al as electrodes. In all of these tests the sense and magnitude of the charge offset were independent of the type of contact.

The importance of the charge offset phenomenon becomes apparent when the numerous possible applications for GFD's are considered. Under alternating field excitation the graded ferroelectrics acquire static charge, that is ΔD reaches a maximum value. However, in a setup where the GFD is kept at a constant temperature and is shunt by a resistive load, The GFD can deliver continuous power into the resistive load when an ac field is applied across the device. The amount of charge flow is directly proportional to the temperature of the ferroelectric device. A small change in the temperature of the device or surrounding (i.e. heat flow in or out of the device) can be directly detected as a corresponding change in the output power level, thus making the GFD an active device.

Figure 2.3 shows the temperature dependence of hysteresis shift and the effective pyroelectric coefficient for the graded KTN films defined as the change in offset charge stored for a change in temperature. The observed peak value is much greater in magnitude than the conventional pyroelectric coefficient found in the best KTN single crystals and even the best thin film ferroelectric materials.

The charge pumping action and the giant effective pyroelectric coefficient observed in KTN films with gradient in polarization open the way for the development of new and unique devices such as an analogue of the Seeback effect for fast, thin film thermal sensors, heat/electrical energy conversion, 3-terminal charge transfer capacitors "transpacitors" without the thermal noise of transfer resistor "transistor" devices.

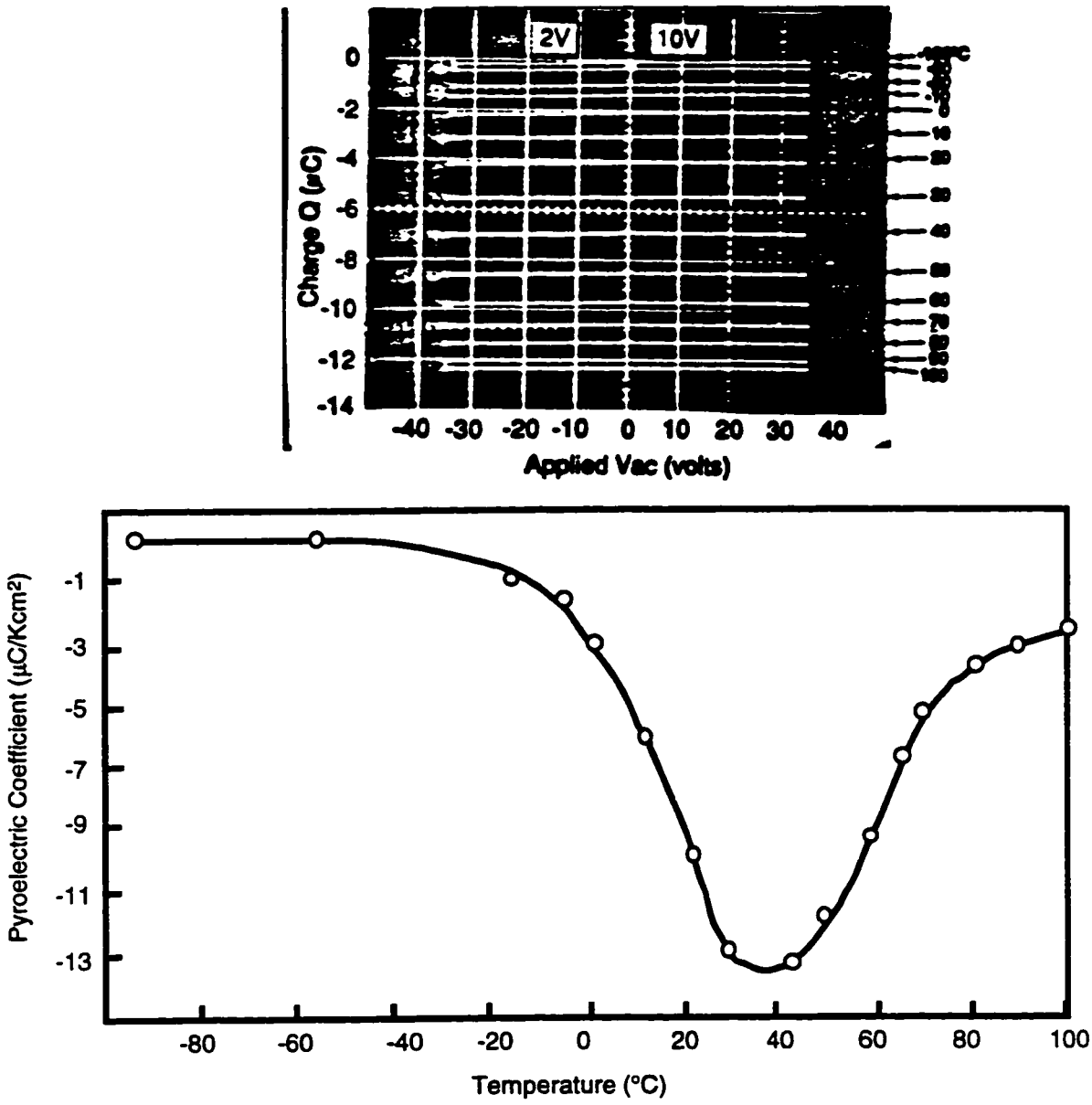

Fig. 2.3: The temperature dependency of (a) the hysteresis shifts and (b) the effective pyroelectric coefficient in 9.8 μm thick graded KTN films

The present work was motivated by the idea of GFD's as the dielectric analogue of transistors and by the wide range of potential applications of GFD's. In the present study, graded ferroelectric devices will be formed from BST thin films using the MOD technique. The GFD-BST systems offer many advantages over the KTN-GFD system. As mentioned before, BST films contain no volatile components which allows for a controlled formation

of a composition gradient throughout the film thickness and not close to the surface only. In addition, the Curie temperature of the BST system can be selected over a wide range of temperature -100°C to 100°C by adjusting the barium to strontium ratio in the films. Also, there are far more applications where barium titanate or BST single crystals and thin films are used than those employing KTN. And finally, the BST system has been extensively studied over the decades and there is numerous number of studies on this system that are available in literature.

Microstructure and Ferroelectric Properties of Fine-Grained $Ba_xSr_{1-x}TiO_3$ Thin Films

3.1: Introduction

The $BaTiO_3$-$SrTiO_3$ system is of considerable interest to researchers in the fields of electro-ceramics and microelectronics. Besides being used in the manufacture of capacitors and thermistors, passive devices based on $BaTiO_3$-$SrTiO_3$ solid solutions are now being considered for use in various new applications, such as in phased array antennas, capacitor-varistor protection devices for microelectronic circuits[1], and uncooled pyroelectric IRFPAs (infrared focal plane arrays) for low cost IR imaging.[2] The high electrical charge storage capacities of $Ba_xSr_{1-x}TiO_3$ (or BST) thin films also make them attractive for on-chip integrated circuit (IC) capacitors and in dynamic random access memory (DRAM) cells.[3-6]

BST films were used in this study in the formation of graded ferroelectric devices (GFDs). Barium strontium titanate was selected in the formation of GFD structures because: barium strontium titanate has low dissipation, has been studied extensively in bulk form, displays ferroelectric hysteresis at near room temperature, and because the ferroelectric phase temperature region can be controlled by adjusting the barium to strontium ratio. At room temperature $Ba_xSr_{1-x}TiO_3$ is ferroelectric when the Ba content x is in the range of 0.7 to 1.0 and paraelectric when x is in the range of 0 to 0.7.[8] Films with polarization gradients have also been examined theoretically.[9]

Before attempting to introduce a model that predicts the properties of BST GFDs, a careful investigation of the electrical and structural characteristics of each of the BST compositions and layers that form the graded structure is needed. Specifically, it is

essential to obtain a clear understanding of the dependencies of the relative permittivity, dissipation, polarization and resistivity on composition x and measurement temperature.

In this chapter, the preparation of $Ba_xSr_{1-x}TiO_3$ thin films by metalorganic decomposition (MOD) is described. The Ba content was x=0.7, 0.8, 0.9 and 1.0. The microstructure and ferroelectric properties were examined as a function of temperature in the range of 0 - 100°C. The grain size for all compositions was in the submicron range, which explains the absence of both a peak value in the relative permittivity and a transition from a ferroelectric to a paraelectric state in the hysteresis loops.

3. 2 : Experimental

Barium strontium titanate (BST) films were prepared using the metalorganic decomposition method (MOD); a simple, low cost and easily controlled technique for making thin films.[10] The MOD process is outlined schematically in Fig. 3.1. Separate solutions of $BaTiO_3$ and $SrTiO_3$ were prepared from superconductor grade barium and strontium neodecanotes (solid), and titanium (IV) 2-ethylhexoxide (liquid). The chemicals were combined in the proper proportions to obtain the desired stoichiometric balance. Xylene and neodecanoic acid were added to obtain a viscosity in the range of 4-6 cps in order to maintain the consistency of the metalorganic solution. Three other solutions were prepared by mixing the proportionate amounts from the original solutions ($BaTiO_3$ and $SrTiO_3$). The compositions of the resulting films were determined by electron probe microanalysis, yielding $BaTiO_3$, $Ba_{0.89}Sr_{0.15}TiO_3$, $Ba_{0.81}Sr_{0.24}TiO_3$, and $Ba_{0.73}Sr_{0.34}TiO_3$. For this analysis, high quality $SrTiO_3$ single crystals and reagent grade sintered $BaTiO_3$ pellets were used as calibrations standards. Film composition was accurate to about 2%.

Each of the homogeneous $Ba_xSr_{1-x}TiO_3$ films was prepared by dispensing the

metalorganic solution onto a platinum substrate (2 cm x 2 cm) which was then spun at a rate of 4000 rpm for 30 seconds. The remaining solvent in the film was removed by placing the film and substrate on a hot plate set to 150°C surface temperature for 2 minutes. Pyrolysis was done in air inside a conventional moffle furnace set to 600°C for 3 minutes. It was necessary to make multiple film depositions in order to obtain the desired final film thickness; which was determined with a thin film profilometer after selective etching in buffered HF. Final film annealing was carried out in flowing oxygen at 1000°C for 60 minutes.

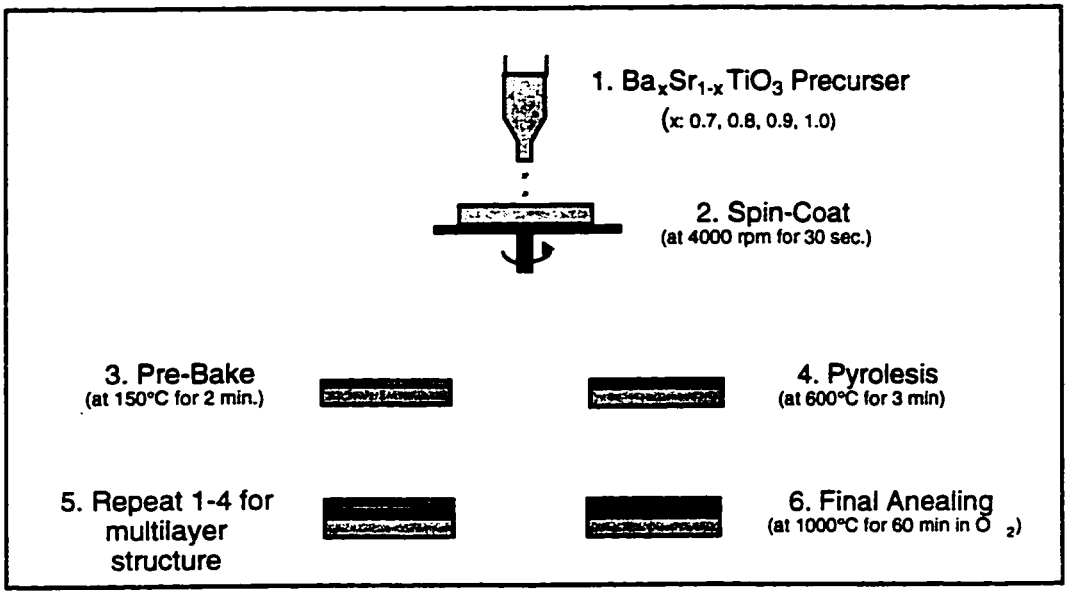

Fig. 3.1: The metalorganic decomposition process

The film microstructure was determined with a computer-controlled Siemens x-ray Diffraktometer using Cu K α (λ = 0.1542 nm) radiation. Surface morphology of each film was determined by scanning electron microscopy (SEM). Electrical measurements were made possible by depositing 0.02 cm^2 gold/chromium circular electrodes onto each film by e-beam evaporation. Each electrode consisted of a 600 Å-thick chromium layer followed by a 3000 Å-thick gold layer.

The platinum substrate served as the counter electrode, as shown in Fig. 3.2.

Capacitance and dissipation versus temperature for the annealed films were measured, under vacuum, with a Hewlett-Packard 4172A analyzer impedance meter using a 1 kHz-1.0 V_{rms} sine wave as a test signal. Direct current resistivity measurements were made under vacuum with a Keithly model 617 electrometer.

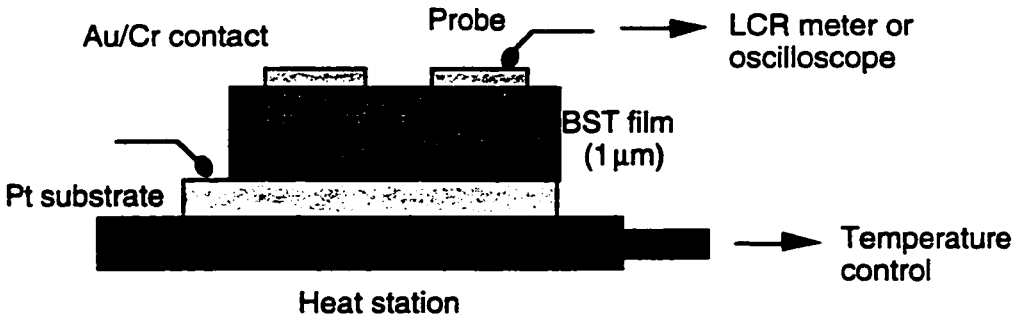

Fig. 3.2 : Diagram of the setup for elctrical and dielectrical measurements

Figure 3.3 shows the basic elements of a modified Sawyer-Tower hysteresis circuit used to measure the spontaneous polarization (P_s), remnant polarization (P_r) and the coercive field (E_c) at various frequencies and excitation levels. The temperature was regulated to within ± 0.05 °C using a low temperature microprobe station. The above measurements were carried out as a function of temperature in the range -40 to 100 °C.

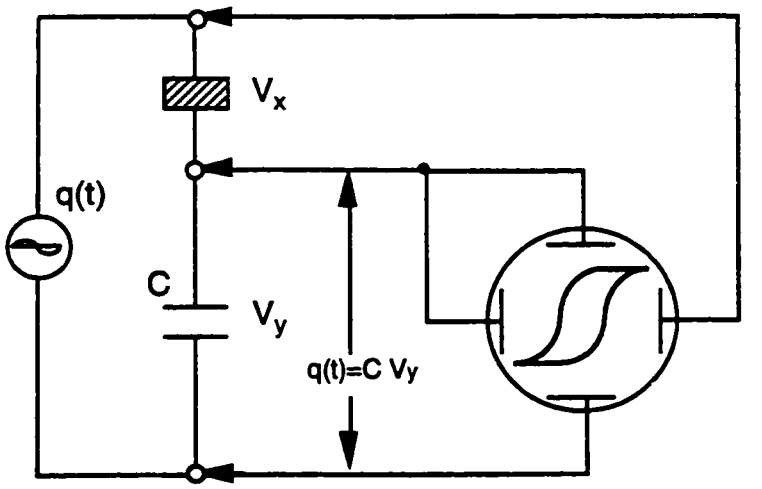

Fig. 3.3 : Elements of the test circuit: Modified Saywer-Tower circuit

3. 3: Results and Discussion

Figure 3.4 shows the x-ray diffraction patterns at room temperature for the BST films as the Ba content (x) was decreased from 1 to 0.7. The $BaTiO_3$ pattern, Fig 3.4a consisted of $BaTiO_3$ and platinum peaks only. No minority phases such as $BaCO_3$ or TiO_2 were observed. The BST films have a tetragonal crystal structure. The d spacing of the BST films are compared with the standard tetragonal $BaTiO_3$ d spacing in Table 3-I.

Tetragonal $BaTiO_3$		$Ba_xSr_{1-x}TiO_3$			
standard		[x=0.73]	[x=0.81]	[x=0.89]	[x=1.0]
hkl	d (Å)	d(Å)	d(Å)	d(Å)	d(Å)
100	3.990	3.963	3.979	3.978	3.980
110	2.825	2.801	2.810	2.818	2.818
111	2.314	2.289	2.295	2.302	2.303
200	1.997	1.981	1.986	1.992	1.991
210	1.786	1.772	1.777	1.783	1.784
211	1.634	1.617	1.623	1.628	1.630
220	1.412	1.402	1.407	1.411	1.411
c/a	1.012	0.998	1.005	1.006	1.016

Table 3-I. D spacing and c/a values for bulk $BaTiO_3$ and BST films with different Sr:Ba ratios.

As the Sr content was increased, there was a corresponding shift in $BaTiO_3$ x-ray diffraction lines towards lower values of d spacing. These shifts are due to the difference in size between the Ba^{+2} ions (r=1.35 Å), and the Sr^{+2} ions (ρ=1.13Å) since both $BaTiO_3$ and $SrTiO_3$ crystallize to the same perovskite structure. The c/a values for the BST films were estimated from the relative intensities of the (200) and (211) x-ray reflections[11].

For $Ba_{0.73}Sr_{0.34}TiO_3$ the c/a ratio was 0.998 which indicates that the film has cubic structure at room temperature. The c/a ratio increases with increasing Ba content and for $BaTiO_3$ it was 1.016; close to the c/a value of 1.012 for bulk $BaTiO_3$.[12]

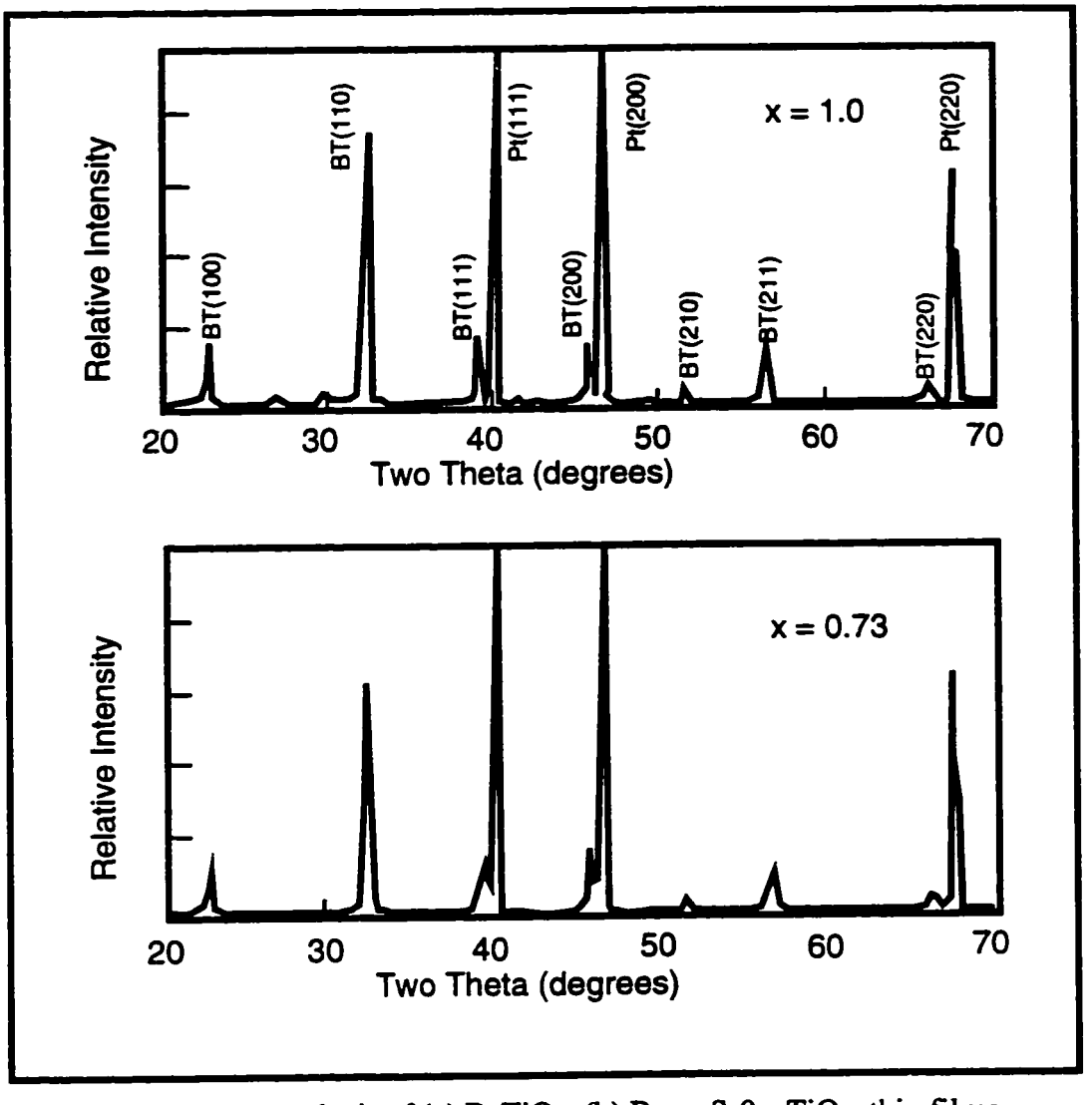

Fig. 3.4:. X-Ray analysis of (a) $BaTiO_3$, (b) $Ba_{0.73}Sr0_{.34}TiO_3$ thin films

The SEM micrographs, Fig. 3.5, reveal the films to be polycrystalline, crack free and of uniform size grains. The grain sizes were estimated from the SEM micrographs using the intercept method. The grain size of all films was in the submicron range and decreases with increasing Sr content. The film thickness and the grain size of each of the BST films are listed in Table 3-II.

	$Ba_xSr_{1-x}TiO_3$			
	[x=0.73]	[x=0.81]	[x=0.89]	[x=1.0]
Film thickness (μm)	1.40	1.50	1.30	1.50
Grain size (μm)	0.05±0.01	0.06±0.01	0.07±0.01	0.08±0.02

Table 3-II: Film thickness and grain size of the $Ba_xSr_{1-x}TiO_3$ thin films.

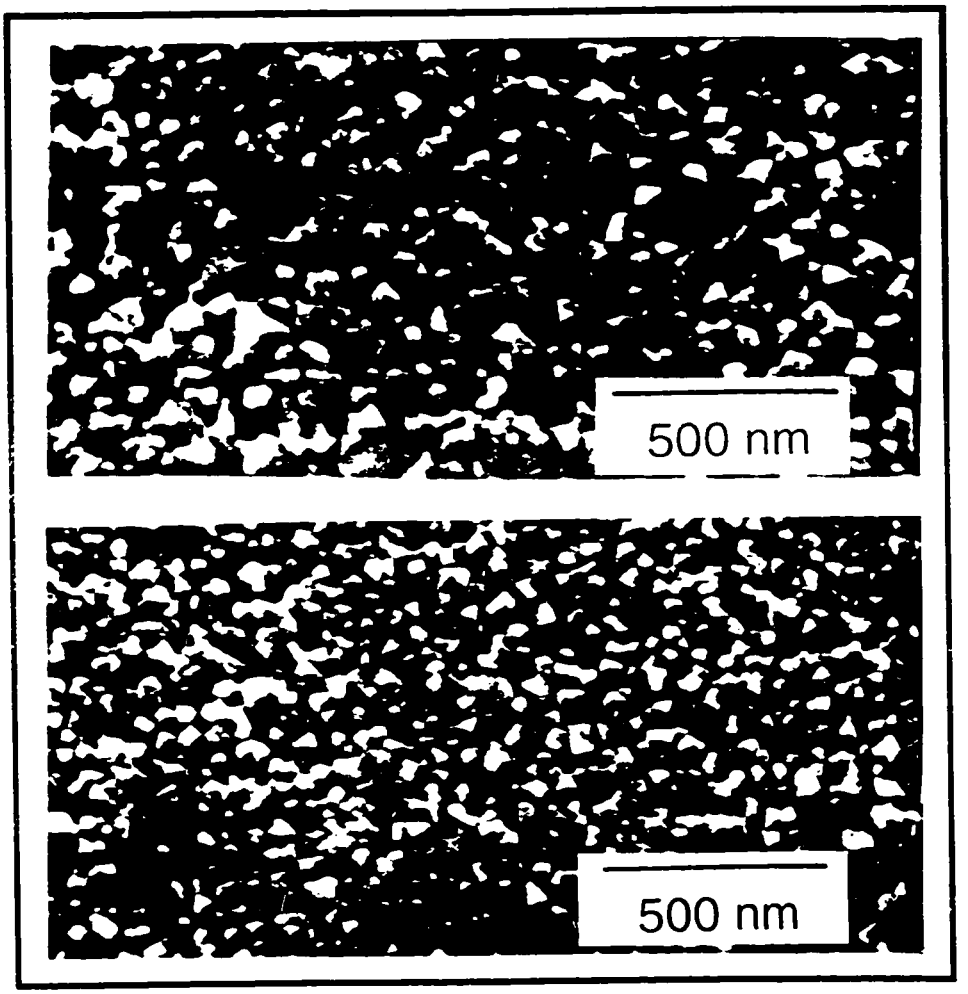

Fig. 3.5: Scanning electron micrographs of (a) $BaTiO_3$ thin films (b) $Ba_{0.73}Sr_{0.34}TiO_3$

Figure 3.6 shows the hysteresis loops for the BST films taken at room temperature with a 1 kHz sine wave and an applied voltage of 30 V_{rms} across the films;

the maximum field strength possible before an electric breakdown of the films. The $Ba_{0.89}Sr_{0.15}TiO_3$, $Ba_{0.81}Sr_{0.24}TiO_3$, and $Ba_{0.73}Sr_{0.34}TiO_3$ films exhibited narrow ferroelectric hysteresis loops with little spontaneous polarization, while better defined hysteresis loops were obtained for the $BaTiO_3$ film due to its relatively larger grain size.

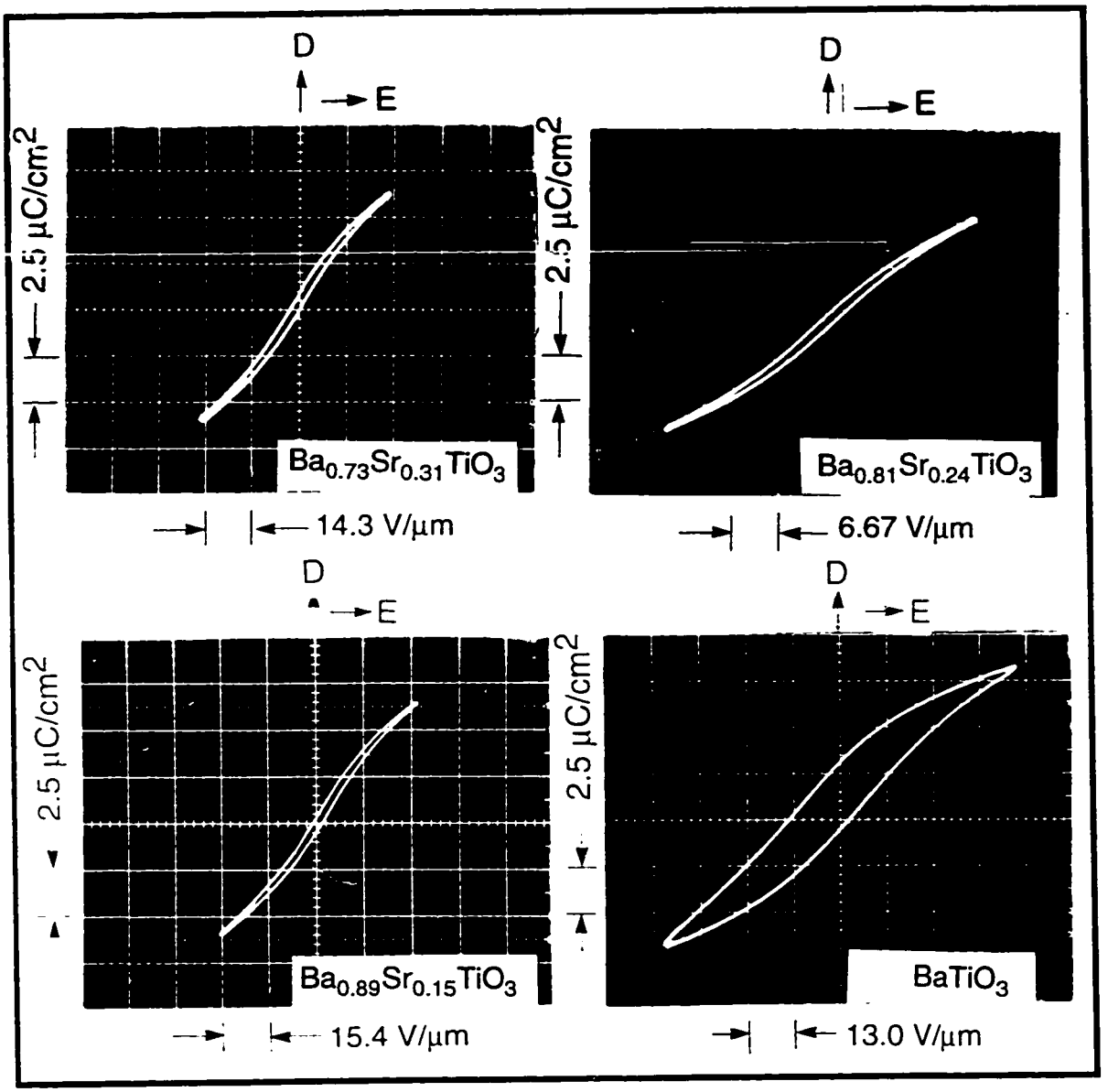

Fig. 3.6 : Polarization versus electric field for the $Ba_xSr_{1-x}TiO_3$ thin films

No transition from the ferroelectric state to the paraelectric state was observed for any of these compositions as the temperature was varied between 0 and 100 °C.

However, it is true that the maximum applied field ($\approx 10^5$ V/cm) is quite high and hence the observed loops for x=0.73 may be the results of a field induced transition from the paraelectric to ferroelectric state.[13,14] The spontaneous polarization (P_S), remnant polarization (P_r), coercive field (E_C) and squarness ratio (s. r.) values were estimated from the hysteresis loops at various temperatures and are listed in Table 2-III.

At room temperature the spontaneous polarization for the $BaTiO_3$ film was 2.8 $\mu C/cm^2$ (0.028 C/m^2). Although this value is less than the 25 $\mu C/cm^2$ (0.25 C/m^2) value typically observed for bulk $BaTiO_3$ ceramic, it is comparable to the spontaneous polarization values observed for films with similar grain size values. J. Xu et al[15] reported a spontaneous polarization value of 1.3 $\mu C/cm^2$ (0.013 C/m^2) for films with grain size of 0.1 μm prepared by MOD. Both values are smaller than the predicted[16] value of 4.75 $\mu C/cm^2$ (0.0475 C/m^2) for randomly oriented polycrystalline $BaTiO_3$ films

Figure 3.7 is a plot of the relative permittivity $\varepsilon_r \equiv \varepsilon/\varepsilon_o$ where ε_o is the permittivity of free space and dissipation factor (tan δ) versus temperature for the BST films. In general, films with non-zero Sr content have higher dielectric constant and smaller dissipation than the $BaTiO_3$ films. For the $BaTiO_3$ film there was a corresponding increase in relative permittivity and dissipation as the temperature increased reaching maximum values of 195 and 0.06 respectively at 100 °C, consistent with what has been observed in ferroelectric thin films[4]. It should be noted, however, that for $BaTiO_3$ thevariation in ε_r between 0 and 100°C did not exceed 10%, while the dissipation nearly doubled within the same temperature range. On the other hand, BST films with x = 0.73, 0.81 and 0.89 showed a continuous decrease in ε_r between 0 and 100°C while tan δ remained essentially constant.

		$Ba_xSr_{1-x}TiO_3$ [x=0.73]	[x=0.81]	[x=0.89]	[x=1.0]
T = 0 °C	ε_r	350	400	310	180
	Tan δ	0.017	0.019	0.018	0.030
	P_r *	0.8	0.5	0.6	1.8
	P_s *	3.8	2.5	2.0	5.5
	E_c +	1.4	1.3	1.4	9.0
	s. r.	3.7	1.7	1.7	4.8
T = 25 °C	ε_r	330	380	310	186
	Tan δ	0.016	0.018	0.019	0.036
	P_r	0.5	0.5	0.8	1.8
	P_s	2.5	2.5	1.8	2.8
	E_c	1.4	1.3	1.4	9.0
	s. r.	2.4	1.1	1.6	4.2
T = 50 °C	ε_r	300	360	300	190
	Tan δ	0.016	0.018	0.019	0.04[illegible]
	P_r	0.5	0.5	0.5	2.0
	P_s	3.0	2.3	2.2	5.0
	E_c	1.4	1.3	1.4	9.0
	s. r.	2.3	1.9	1.8	4.6
T = 100°C	ε_r	260	310	280	195
	Tan δ	0.016	0.022	0.021	0.057
	P_r	0.5	0.4	0.5	
	P_s	3.0	1.5	2.0	Short
	E_c	1.4	1.3	1.4	Out
	s. r.	3.0	1.7	1.9	

(* Units are $\mu C/cm^2$) ($^+$ Units are V/μm)

Table 3-III: Relative permittivity (ε_r), loss tangent (Tan δ), remnant polarization (P_r), spontaneous polarization (P_s), coercive field (E_c), squarness ratio (s. r.) of $Ba_xSr_{1-x}TiO_3$ thin films annealed at 1000 °C for 60 min. in oxygen.

Figure 3.8 and Table 3-III show that at room temperature, a maximum value for the relative permittivity of 380 was obtained for x=0.81 and a minimum dissipation value of 0.016 was obtained for x=0.73.

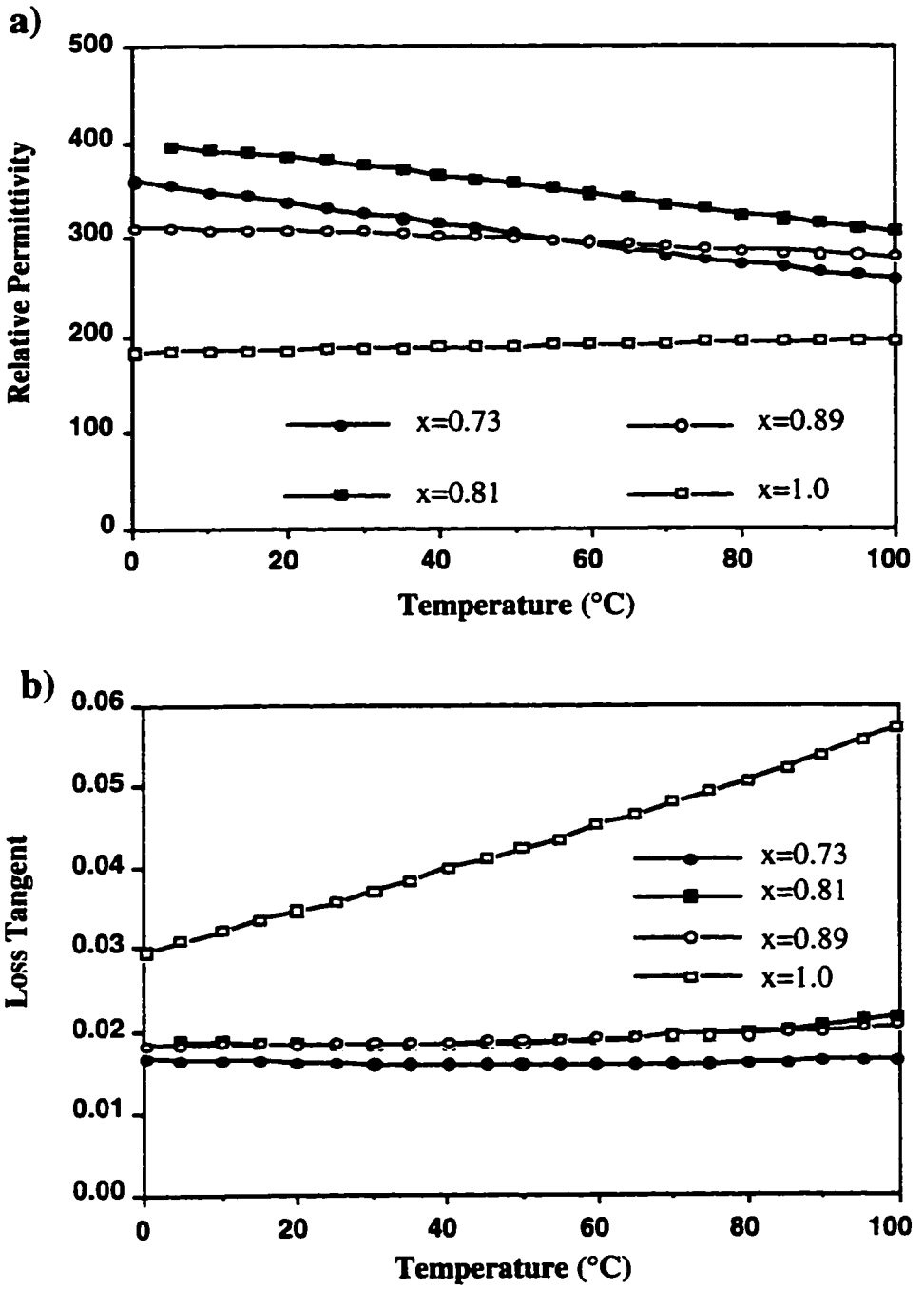

Fig. 3.7: (a) Relative permittivity and (b) dissipation factor as a function of temperature for $Ba_xSr_{1-x}TiO_3$ thin films annealed at 1000 °C for 60 min. in oxygen.

Measurements of the dc resistivity have shown that for all compositions there was a decrease in resistivity with increasing temperature. At room temperature the dc. resistivity was maximum for $Ba_{0.73}Sr_{0.34}TiO_3$ (ρ = 3.0 TΩ–cm) and minimum for

$BaTiO_3$ (ρ = 0.6 TΩ-cm). At all temperatures the dc resistivity was greater than 70 GΩ-cm; therefore it is fair to conclude that contribution of the electronic conductivity to the dissipation factor is minimal and can be ignored at practical frequencies.

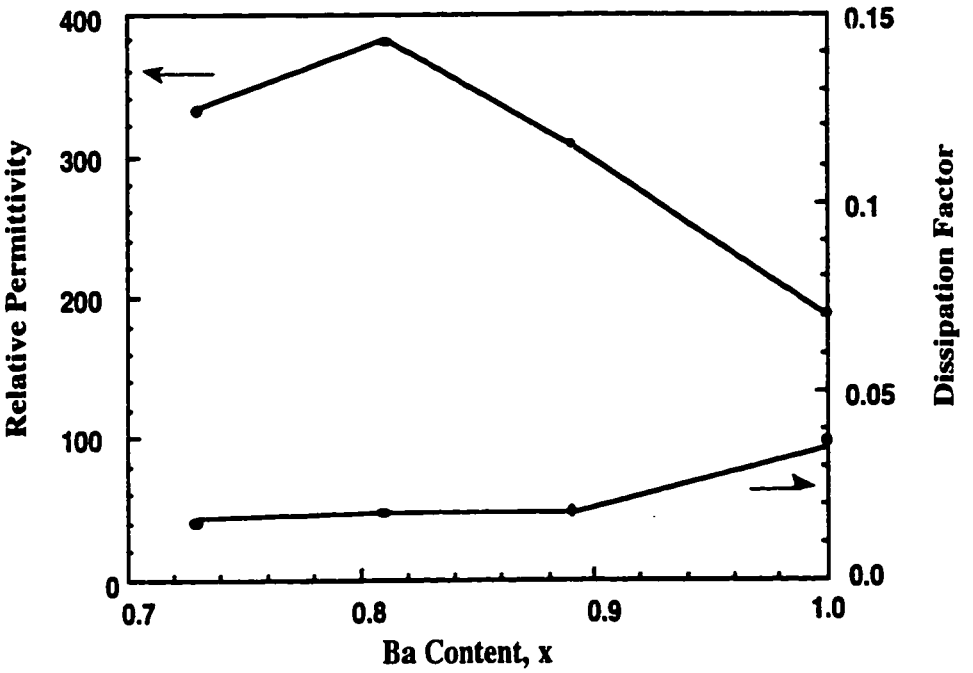

Fig. 3.8: Relative permittivity and dissipation factor at room temperature as a function of composition x for the $Ba_xSr_{1-x}TiO_3$ thin films.

It was not possible to determine a Curie temperature for any of the films under study as none of the films showed a maximum value in the ε_r versus temperature plot. However, since the dielectric constant of the $BaTiO_3$ film showed a monotonic increase with temperature we can not rule out that a peak in ε_r may exists at a temperature higher than 100 °C, which is the maximum temperature attainable in the temperature microprobe station used in our study. J. Xu et al [15] have shown that for the 0.1 μm film a broad maximum in ε_r appeared at $T_c \approx 130$ °C. For smaller grain sizes ε_r remained constant and was not affected by the variation in temperature.

The dependence of ε_r on temperature observed in our study is consistent with the

results obtained by Miyasaka et al [17] for BST thin films with thicknesses between 0.4 and 0.5 μm. The films were prepared by rf-sputtering and annealed at different temperatures. Their results show that for $BaTiO_3$, ε_r slightly increased with increasing measurement temperature. For all other compositions ε_r decreased with increasing temperature. They also noted that a peak in ε_r versus temperature occurred only for x=0.5. In our results, the absence of a peak value in the relative permittivity versus temperature and a distinguishable transition from the ferroelectric state to the paraelectric state in the hysteresis loops can be explained by the difference in structure between grain boundaries and grain bulk. Grain boundaries are amorphous in nature and thus have lower dielectric constant than the grain bulk. Therefore a decrease in the grain size results in an increase of the fraction of amorphous volume relative to the amount of crystalline forms present in the material and consequently an overall decrease in the spontaneous polarization and dielectric constant of the sample. Previous studies [16-21] reported that a minimum grain size of 0.5 μm was necessary in order to observe a peak in ε_r. It was also shown that the ferroelectric properties of $BaTiO_3$ were greatly enhanced when the grain size approached 1 μm.

Chapter 4

Slater Model for Graded Ferroelecric Devices

4.1: The Model

In this chapter, Slater's empirical model for ferroelectric materials has been extended to also describe thin films with polarization gradients normal to the growth surface, i.e., graded ferroelectric devices (GFD's). This model accounts for several aspects of these structures, including: the broadness of the permittivity plots with temperature, the formation of a spontaneous potential upon oscillatory field excitation, offsets in the hysteresis graphs along the displacement axis with directions which are gradient dependent, and the electric field dependence of that offset.

While polarization variable heterostructures, whether from strain induced origins[1,2] or compositional variations[3,4] are of growing interest, their formation has been to date primarily an artifact of their growth process rather than through design. In addition, though a heuristic model which accounts for the observed steady-state behavior in compositionally graded structures has been proposed[4], it is incomplete as it fails to account for the dynamic responses of the structures arising from external stimuli (particularly field dependence), nor does it quantify those properties which it does consider. Also, previous theoretical considerations do not provide a formalism for predicting new phenomena which might then be discovered.

In this chapter a microscopic model for graded ferroelectric materials based upon energy considerations was developed according to the methodology first proposed by Slater[5-7]. This model accounts qualitatively for the known properties of graded ferroelectric devices (GFD's), particularly: the broadness of the permittivity plots with temperature, the formation of a spontaneous potential upon oscillatory field excitation, and

the electric field dependence of the new hysteresis phenomenon[3,4].

Slater proposed[5-7] that the energy function for a ferroelectric material could be written as:

$$\mathcal{E} = k_o(T - T_c)x^2 + Bx^4 \qquad (4.1)$$

Here, x, is the ion displacement relative to a central charge, T and T_c are the absolute and Curie temperatures respectively, and k_o and B are characteristic functions of the ferroelectric material; these latter quantities being functions of temperature as well.

Such a potential implies a ferroelectric state when the temperature falls below the critical temperature, T_c. For $T < T_c$, extrema in the energy exist at $x = 0$ and also at $x = \pm\sqrt{\frac{k_o(T_c - T)}{2B}}$, the latter corresponding to the two spontaneous polarization states of the ferroelectric dipoles, as shown in Fig. 4.1. We can immediately write an expression for the spontaneous polarization, P_S, as: $P_S = Nq\sqrt{\frac{k_o(T - T_c)}{2B}}$. Where, q, is the ionic charge and N is the number of dipoles per unit volume.

If $\mathcal{E}$ is expanded about $x - \sqrt{\frac{k_o(T - T_c)}{2B}}$, with only terms second order in $x - \sqrt{\frac{k_o(T - T_c)}{2B}}$ kept, we have:

$$\mathcal{E} = \Delta\mathcal{E} + \frac{1}{2}\left(x - \sqrt{\frac{k_o(T_c - T)}{2B}}\right)^2 4k_o(T_c - T) \qquad (4.2)$$

where $\Delta\mathcal{E} \equiv -\frac{(k_o(T_c - T))^2}{4B}$ is the relative depth of the energy potential at $x = \pm\sqrt{\frac{k_o(T_c - T)}{2B}}$.

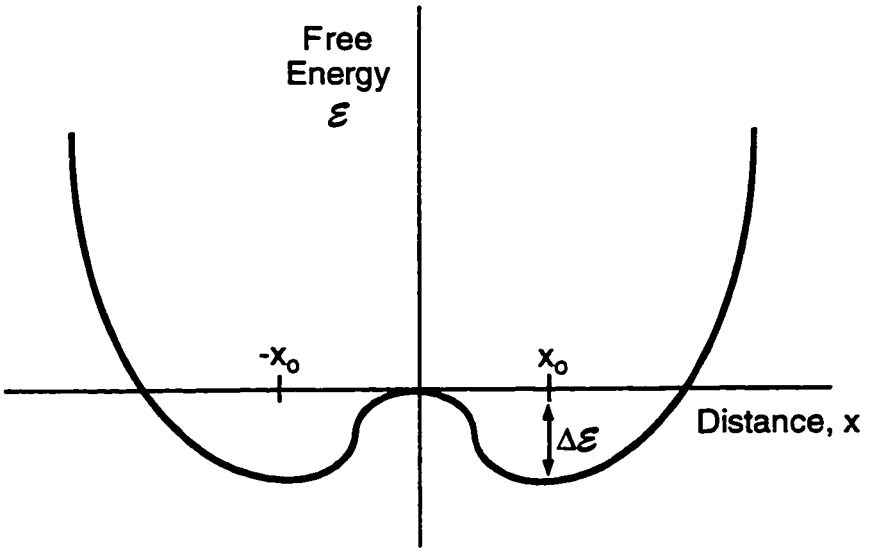

Fig. 4.1: Expanded view of the ferroelectric energy diagram for T<Tc

P_S is related to the energy function through the permittivity as further described by Slater[5,6,8], where the Lorentz-Lorentz correction for the local dipolar field must be included. Thus $\Delta\mathcal{E}$ can be rewritten as:

$$\Delta\mathcal{E} \equiv -\frac{P_S^2}{24N\varepsilon_o} \tag{4.3}$$

where ε_o is the permittivity of free space. Equation (4.3) is our most important result in that it sets the energy scale relative to the spontaneous polarization.

For a large group of perovskite-type ferroelectric materials[9,10], the permittivity, ε, and P_S are approximately linearly related to the composition, c. Here ε is defined by the relation $\varepsilon \equiv (\partial D/\partial E)_{E=0}$, where D is the electric displacement, and E is the electric field. For a linearly graded composition normal to the growth surface:

$$P_S = P_S(c_o)\cdot\left(1+\frac{z}{c_o}\nabla c\right) \tag{4.4}$$

and

$$\varepsilon = \varepsilon_o(c_o)\cdot\left(1+\frac{z}{c_o}\nabla c\right) \tag{4.5}$$

where $P_S(c_o)$ and $\varepsilon_o(c_o)$ may be temperature[11-14] and, in a polycrystalline material, field[15,16] dependent. Here c_o is the composition at some reference plane along the composition gradient and z is the normal distance as measured from the film/substrate interface.

We can immediately see that $\Delta\mathcal{E}$ varies as:

$$\Delta\mathcal{E} = -\frac{P_S^2(c_o)\cdot\left(1+\frac{x}{c_o}\nabla c\right)^2}{24N\varepsilon_o} \tag{4.6}$$

or that to first order in the composition gradient there exists a "built in" potential difference:

$$V_S = \frac{P_S^2(c_o)\frac{t}{c_o}\nabla c}{12eN\varepsilon_o} \tag{4.7}$$

across the device (with t the thickness of the material, and e the electronic charge) when $T << T_c$ for all compositions along the grade. $\mathcal{E}$ will then take the form of a series of double potential wells linearly skewed (for linear grade) due to the compositional gradient, as shown in Fig. 4.2. Thus, $\Delta\mathcal{E} = eV_S$, has the same positional functional dependence as the energy function of a poling potential applied to a conventional ferroelectric material[5], a result previously conjectured to be true[5] but now shown to be a result of the Slater formalism for GFD's.

In thin film ferroelectric materials the spontaneous and remnant polarizations are often functions of applied external field, never quite saturating prior to exceeding the breakdown strength of the material[15-16]. In a hysteresis plot of electric displacement as a function of field this is characterized by a failure of the function to achieve a final permittivity equal to that of free space.

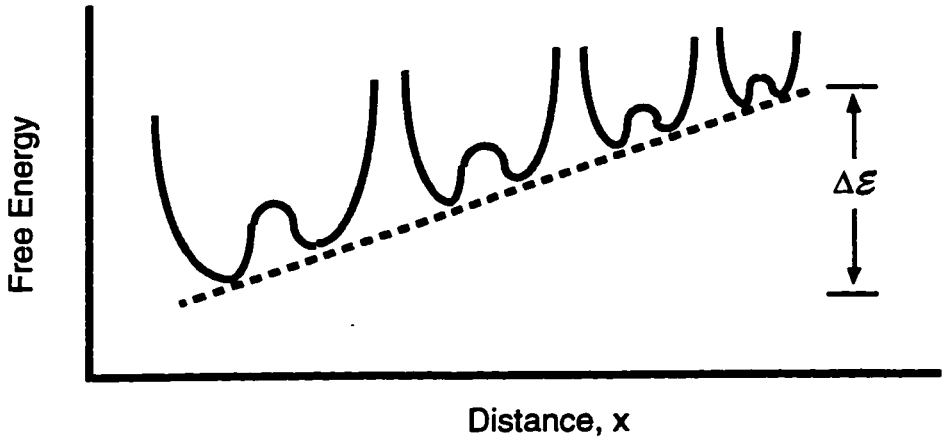

Fig. 4.2: Schematic diagram of the energy as a function of displacement for GFD's

Polycrystalline ferroelectric materials have thus been characterized by a field dependence of the form: $P_S \propto \bar{P}_s(c_o)E_{max}^{\gamma}$, where E_{max}^{γ} is the maximum applied field, γ is typically, but not exclusively, in the range[15,16], $1 \leq \gamma \leq 2$, and is a constant. We can thus rewrite (4.7) as:

$$V_S = \frac{\left(\bar{P}_S(c_o)E_{max}^{\gamma}\right)^2 \frac{t}{c_o}\nabla c}{12eN\varepsilon_o} \qquad (4.8)$$

Equation (4.8) therefore predicts that there should be a spontaneous potential, V_S, which should appear across a GFD upon the application of an oscillatory electric field, E_{max}, which is indeed observed for such devices[4].

Equation (4.8) also implies[5-8] that a traditional Sawyer-Tower[17] measurement of the hysteresis behavior of a GFD should result in a non-symmetric charge offset[3,4], given by $\Delta Q = C_{GFD} \cdot V_S$ where C_{GFD} is the film capacitance, $C_{GFD} = \varepsilon A/t$. Subtituting V_s and C_{GFD} the charge offset can be expressed as:

$$\Delta Q = \frac{\varepsilon A\left(\bar{P}_S(c_o)E_{max}^{\gamma}\right)^2 \frac{\nabla c}{c_o}}{12eN\varepsilon_o} \qquad (4.9)$$

with, A, the area of the GFD.

This offset is not only a function of the excitation field ($\sim E^{2\gamma}$) but is also dependent upon the gradient in polarization (through ∇c) which determines the sign of ΔQ.

4.2: The Two State "Up" and "Down" Graded Ferroelectrics

To test the predictions of the extended Slater model, compositionally graded devices (GFD's) were formed from $Ba_xSr_{1-x}TiO_3$ films by metallorganic decomposition (MOD). Graded structures were fabricated by the successive deposition of barium strontium titanate ($Ba_xSr_{1-x}TiO_3$, BST) layers each approximately 100 nm thick with a range of Ba to Sr ratios, see Figs. 4.3a and 4.3b. Two layers of each composition were deposited by spin-coating the metallo-organics onto 2cm x 2cm platinum foil. The solutions were made from carboxylates of barium, strontium, and a titanium ethoxide in the proportions Ba:Sr:Ti = 1:0:1, 0.9:0.1:1, 0.8:0.2:1, 0.7:0.3:1 dissolved in xylene[15]. For GFD-BST "Down" the $BaTiO_3$ layers were deposited first and the $Ba_{0.7}Sr_{0.3}TiO_3$ layers were deposited last. The order was reversed for GFD-BST "up", i.e., the $Ba_{0.7}Sr_{0.3}TiO_3$ layers were deposited first and the $BaTiO_3$ layers were deposited last.

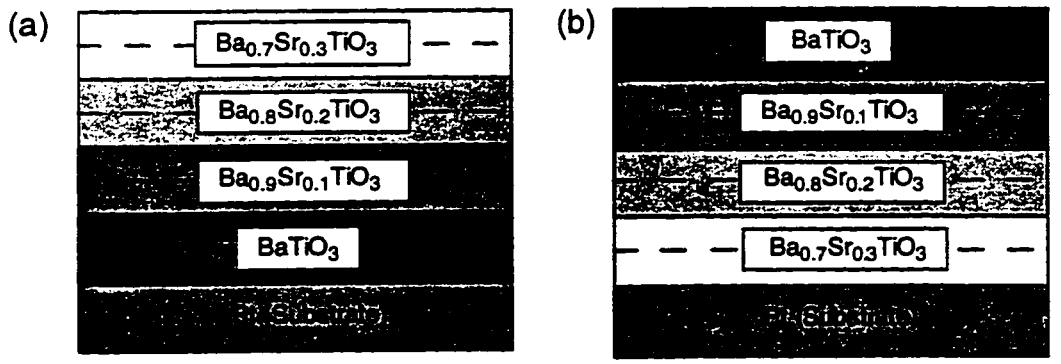

Fig. 4.3: Schematic of the GFD structure prior annealing for (a) GFD "Down" and (b) GFD "Up

The heat treatment procedure for the BST-GFD's slightly differed from that

followed for homogeneous BST films. The first two layers in each structure were deposited and pyrolyzed in a similar manner to homogeneous BST films. The film and substrate were then slowly annealed at 1185 °C over a period of 36 hours. The GFD structure was then completed by depositing the rest of the layers, pyrolizing each layer at 600 °C for 3 minutes, and finally annealing the whole structure at 1100 °C in flowing oxygen for 30 minutes. The reason behind the additional annealing step is to enhance grain growth in the base layers, which function as "seed" for growing large grains in the subsequent deposited layers. The SEM micrographs, Fig. 4.4, show a clear improvemnet in grain size for the two seed layers, $Ba_{0.7}Sr_{0.3}TiO_3$ and $BaTiO_3$, compared to films with the same compostions that were annealed only at 1000 °C.

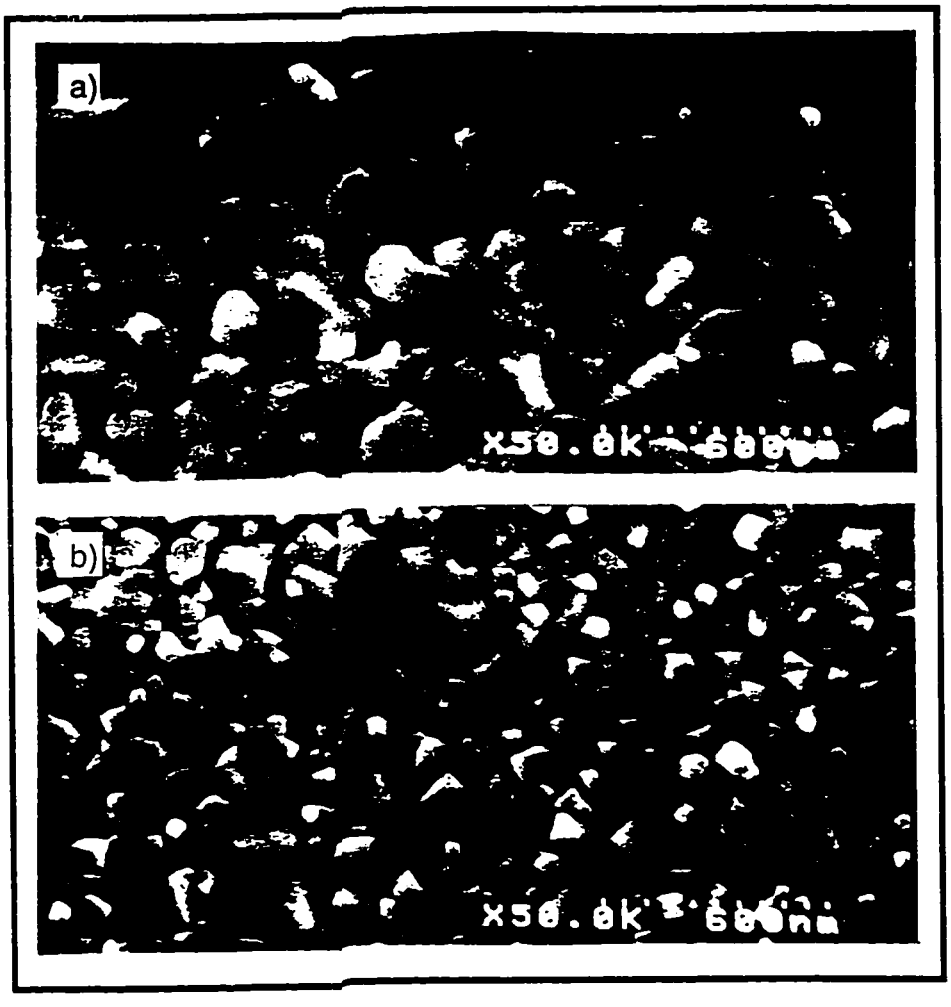

Fig. 4.4: SEM Micrograph of the "seed" layers for (a) GFD "Down" and (b) GFD "Up"

Comparison of the x-ray patterns of the graded structures (Fig 4.5) and the homogeneous stuctures (Fig. 3.4) indicates that while the Pt peaks were unchanged, the BT peaks become more diffused. This is more appaent in the GFD "Up" structure where the $BaTiO_3$ layer is on top.

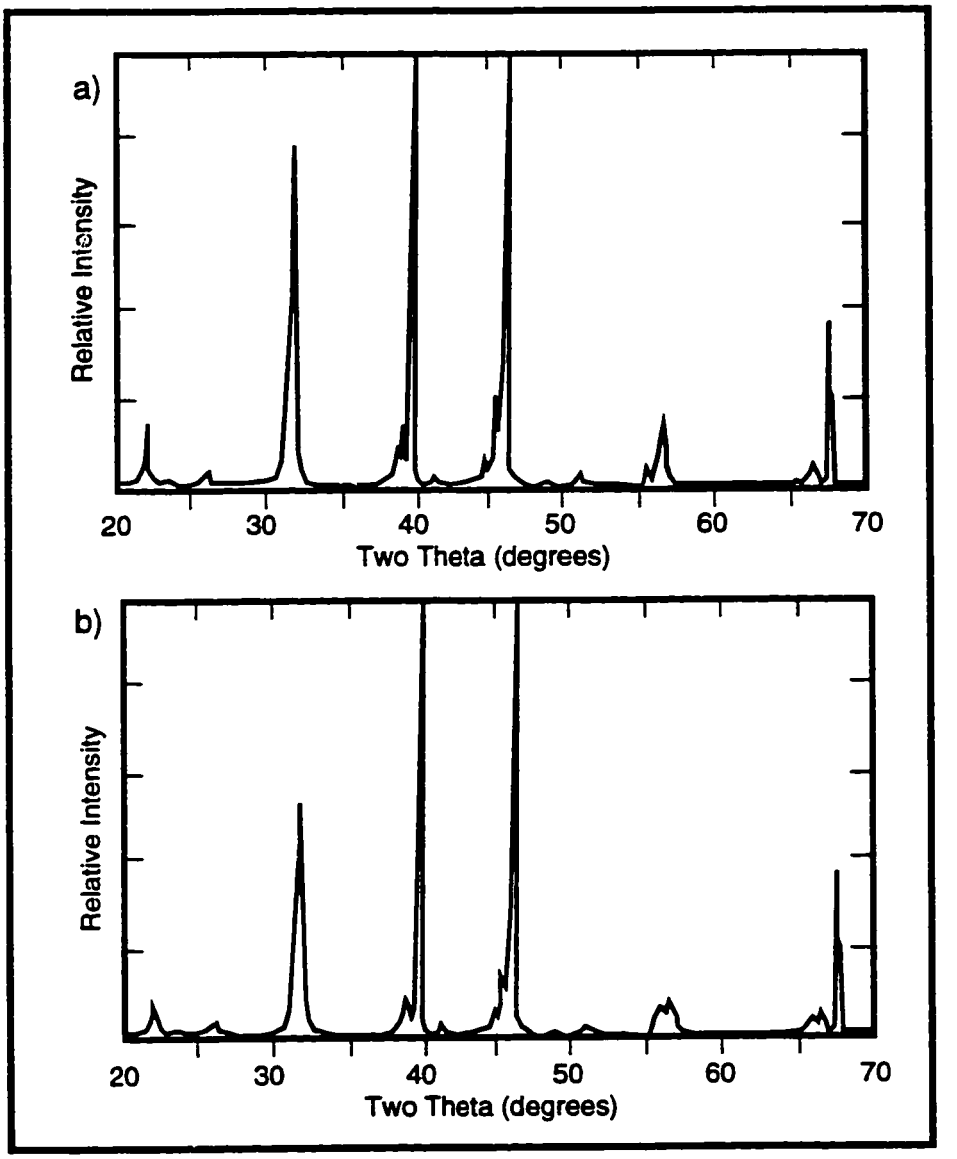

Fig. 4.5: X-ray diffracttion patterns for (a) GFD "Down" and (b) GFD "Up".

Compositional depth profiling, using ion milling and x-ray photospectroscopy, showed that continuous grades, see Figs. 4.6a and 4.6b, had indeed been formed. Elemental compositional depth analysis of the films revealed, respectively, uniformly

increasing and decreasing linear variations in Ba:Sr ratios (with constant Ti content) through the depth of the films. Final film thickness was measured with a Diktak 330 profilemeter and found to be approximately 1.2 μm.

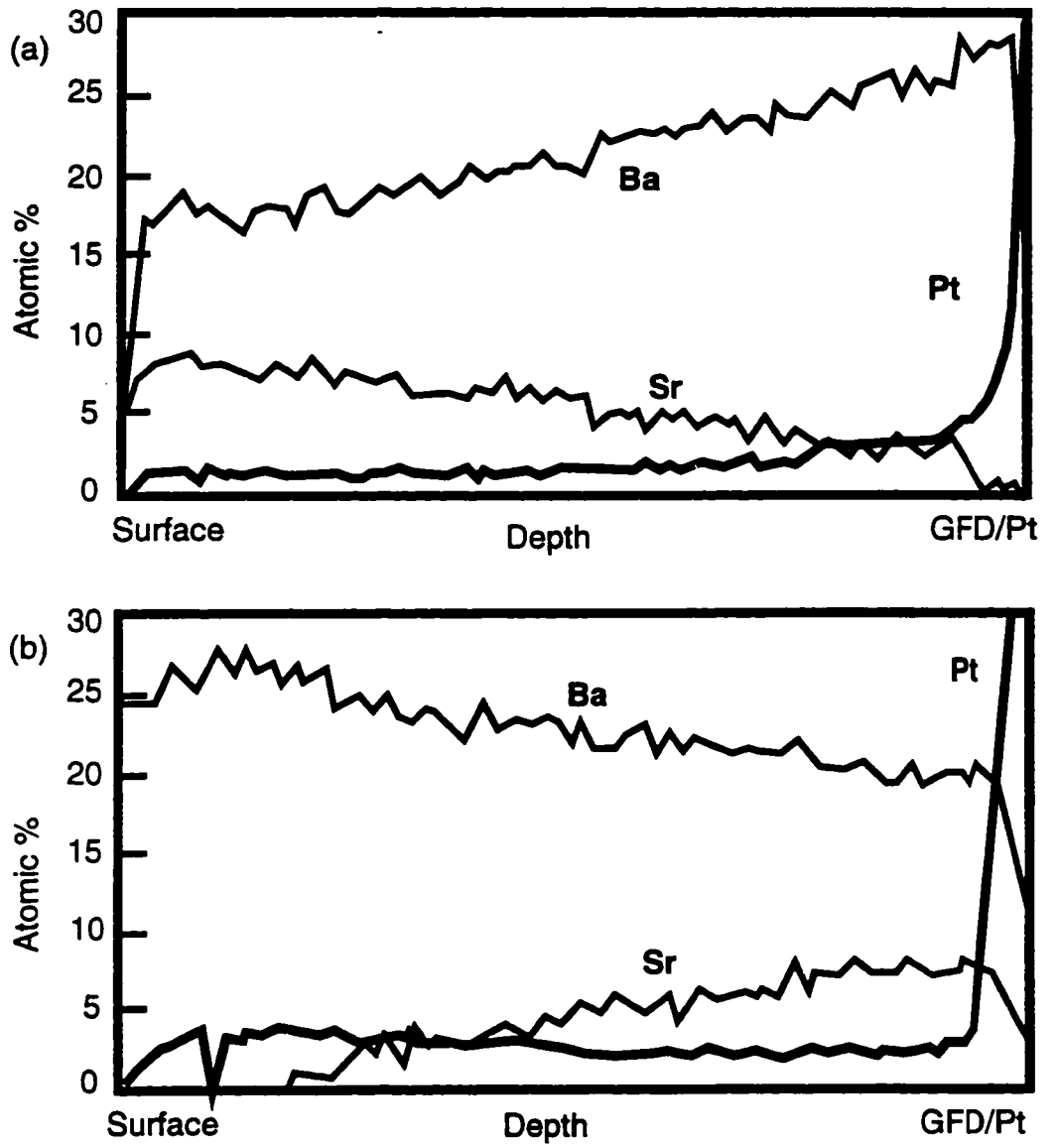

Fig. 4.6: X-ray photospectroscopy chemical profile of (a) GFD "Down" and (b) GFD "Up as a function of depth

Capacitor structures were formed by the subsequent deposition of gold-chrome, 0.02 cm^2, contacts through a shadow mask. The gold was approximately 300 nm thick on 60 nm of chromium. The platinum substrate served as the counter-electrode. Hysteresis measurements were performed under vacuum at room temperature in a temperature

controlled system (stability 0.05 °C) using a modified Sawyer-Tower circuit[17] with 1 kHz sinusoidal voltage excitation.

A plot of the relative permittivity, $\varepsilon/\varepsilon_o$, as a function of field and temperature for the GFD structure described above (Fig. 4.7) reveals a slowly varying function of temperature, showing no dramatic maximum which is characteristic of some large grained ceramic BST materials. While such broad featureless permittivity plots are not uncommon for homogeneous ferroelectric films[3,4,15], particularly BST, the distribution in Curie temperatures which arises from the compositional gradient is known to further smear the cubic to tetragonal ferroelectric transition (with temperature) and thus diminish and further broaden any peak in the permittivity plots. Such effects have been discussed extensively in the literature [3,4,18-20].

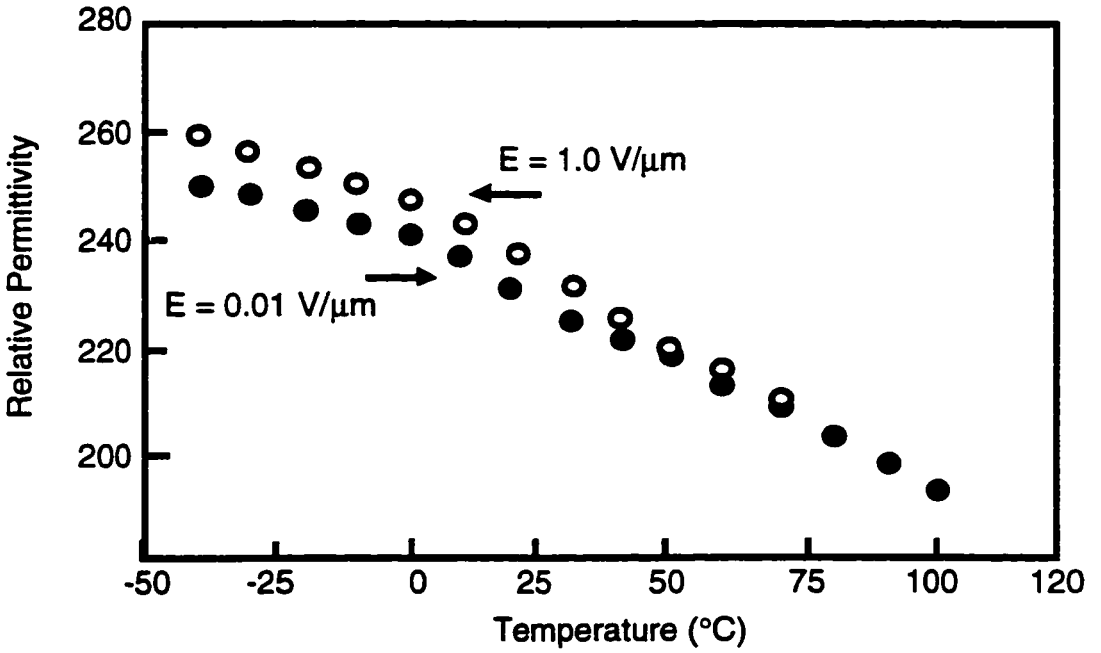

Fig. 4.7: Relative Permittivity, $\varepsilon/\varepsilon_o$, as a function of field and temperature

In contrast to the usual hysteresis phenomenon observed in non-graded ferroelectric materials, Figs. 4.8a and 4.8b show respectively quite distinct "Up" and "Down" translations of the hysteresis loops along the displacement axis with increasing applied

voltage: a new hysteresis phenomenon[3]. In these hysteresis graphs the gain of the amplifier of the displacement voltage has been greatly reduced so as to capture the substantial translational effect, hence the loops appear as flattened lines in the plots. "Up" and "Down" are relative terms in that the platinum substrate was the reference electrode in both hysteresis measurements, hence the sense of the displacements may be reversed by a simple exchange in the position of the reference electrode.

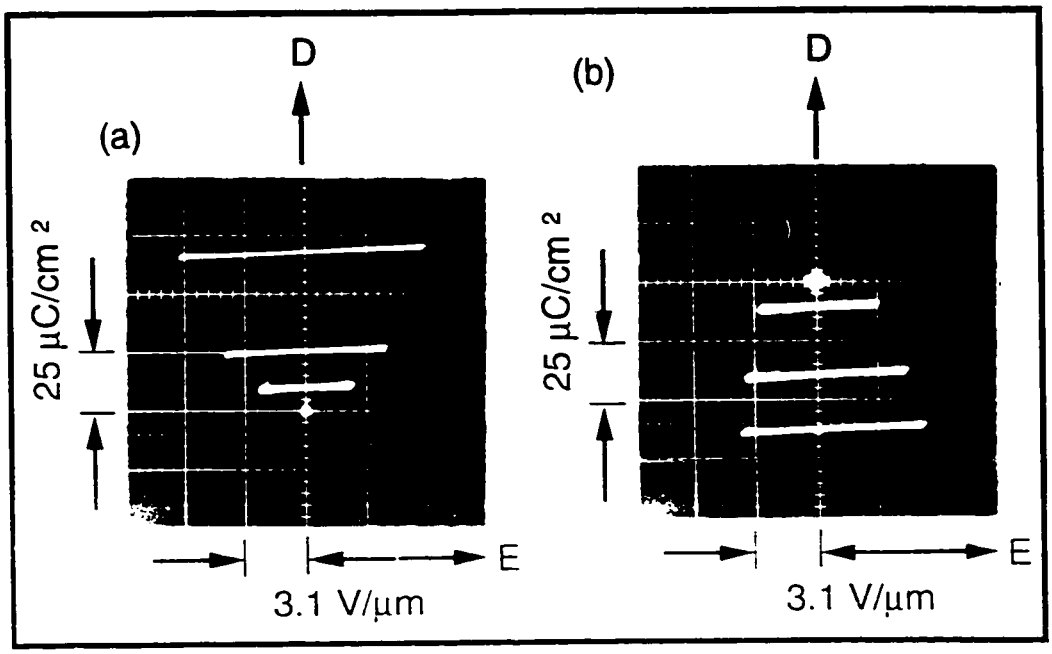

Fig. 4.8: The unconventional hysteresis phenomenon in GFD (a) "Up" and (b) "Down".

Unconventional hysteresis was **never** observed in homogeneous BST capacitor devices formed from uniform composition films for the entire range of starting material compositions, thicknesses, and precursors (Chapter 3). Thus, the response of the GFD's reported in this work cannot easily be attributed to contact or instrumental effects. In addition, because the translations are reversible with reverse grades, though the number and compositions of the layers remain the same, it cannot simply be argued that free ions or electric breakdown are the root causes. Finally, it should be reported that these devices have low and symmetric leakage currents over the range of measured voltages, thus eliminating electric breakdown as a source of the displacement translations.

In Fig. 4.9 we plot P_S as a function of maximum applied field. A best fit to the data indicates that $P_S \propto E_{max}^{\gamma}$, with $\gamma \sim 2.4$. Figure 4.9 also shows the measured field dependence of ΔQ. A best fit to the data indicated that $\Delta Q \sim E^{4.4}$, which compares favorably with the predicted field dependence.

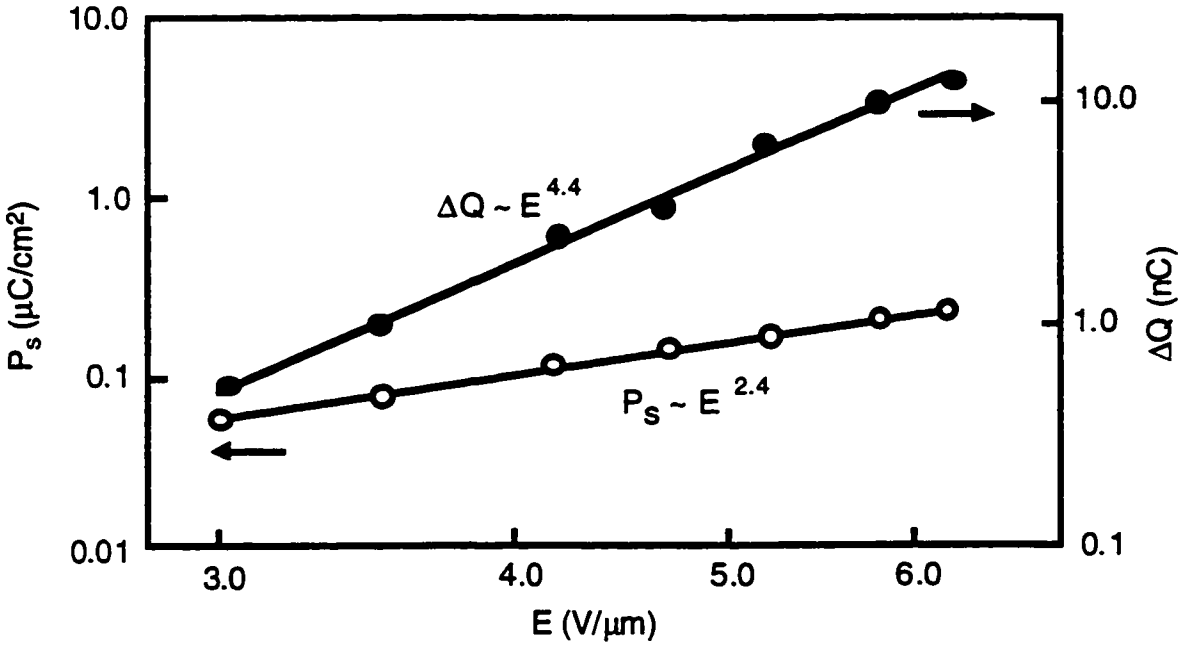

Fig. 4.9: Plot of the spontaneous ploarization, Ps, (○) and charge offset, ΔQ, (●) as a function of maximum field for GFD "down".

We thus see that our expression for the charge offset (4.9), qualitatively accounts for the direction and field dependence of the displacement; though, it dramatically underestimates the magnitude of the offset. One, however, cannot expect to do much better in predicting the magnitude of ΔQ from the Slater-GFD model in its present form. As has been previously pointed out[5,7,8,21,22], such an analysis fails to account for both the electron polarizability and the fact that not all the ions are at positions of cubic symmetry, hence grossly underestimating the magnitude of the Lorentz correction. While we could proceed to account for these factors by a suitable adjustment of the prefactors of charge offset formula, such an analysis would not change the conclusions of this work. Thus our extension of the Slater model for ferroelectric materials to structures with polarization

gradients normal to the growth surface captures the essential features of these devices known to date.

titanate (BST) films were used in the formation of graded ferroelectrics with compositional gradient. The BST system offers the following advantages: it has a simple crystal structure, it is non-toxic, has no volatile components, the Curie temperature can be easily adjusted to any temperature in the range -100 °C and 100°C by controlling the Ba/Sr ratio, and finally BST single crystals and thin films have been extensively used as sensing elements in infrared detection systems. However, one must not rule out other ferroelectric materials such as lead zirconate titanate (PZT) or lead barium titanate (PBT) as starting materials in future GFD's as they may prove to exhibit larger DC hysteresis offsets and hence have a greater pyroelectric sensitivity than BST.

- **Deposition Techniques:** The metallorganic decomposition (MOD) method is a simple, low cost, non-vacuum deposition technique that is capable of producing films with uniform stoichemetry. However, in this study, this method proved to be inadequate to produce films with a smoothly varying gradient in composition. Other deposition techniques with the capability of forming films with true composition gradient at low temperatures such as chemical vapor deposition (CVD), implantation, and sputtering must be considered.
- **Substrates:** In this study platinum foils were used as substrates for graded ferroelectric devices. Platinum was used mainly because it is an excellent conductor (used as the bottom electrode) and because it can withstand the high annealing temperature in the presence of flowing oxygen without changing phase or forming oxides. However, the use of platinum substrate in a mass production of the devices is obviously cost prohibited and therefore other substrates that are compatible with the silicon IC technology must be considered.
- **Other Factors:** The effects of factors such as film thickness, film heat treatment, and the frequency of the applied AC field on the performance of GFD's must be determined beforehand in order to maximize the hysteresis offset and

hence a obtain a maximum pyroelectric sensitivity.

- **Graded Ferromagnetic Devices (?):** The main distinctive feature of graded ferroelectric devices is the existence of an electrical dipole moment (polarization) gradient coupled to a gradient in composition of a ferroelectric material through film thickness. One may envision that based on the duality principle in electromagnetics, graded ferromagnetic devices (or GFD_{μ}) can be easily formed by creating a gradient in composition in a ferromagnetic material which give rise to an associated gradient in magnetic dipole moments (magnetization) through the film thickness. It is expected that these devices exhibit behavior analog to graded ferroelectric devices (GFD_{ε}), however one should not exclude the possibility that these devices may even exhibit new and hitherto unknown or unimagined properties that may one day have very impressive applications.

Appendix A

Metallorganic decomposition (MOD)

A.1: Chemistry of Metallorganics

Metallorganic decomposition (MOD) is a simple non-vacuum liquid -based spin-on method of depositing thin films. This technique is based on decomposition of metallorganics, which are complex coordinate covalent compounds with metal atoms bonded to organic liquid, into a much simpler and more stable form such as the metal itself or its oxide. In metallorganic compounds the metal atom is in the form of a salt and is usually bonded to an oxygen, nitrogen, or sulfur atom but *not* to a carbon atom. Because the metal in the metallorganics exists in a salt form these compounds have low vapor pressure and hence have high degree of stability and at the same time safe and simple to use.

Metallorganic compounds used in MOD are usually prepared in-house and few such as octoates, neodecanoates, amines and mercaptides are commercially available. Of these compounds carboxylates such as neodecanoates and octoates (also known as 2-ethyl-hexanoates) are most commonly used. In a typical carboxylate compound, the metal atom is bonded to a hydrocarbon chain via an oxygen atom. The metal atom species and the length and structure of the hydrocarbon chain determines the solubility, viscosity and volatility of the carboxylate. Fig. A.1 shows the chemical structure of carboxylates, octoates and neodecanoates, where M is a metal atom and R is a hydrocarbon chain. The branched nature of these salts renders greater solubility upon these compounds than would straight chains hydrocarbons[1].

Carboxylates are generally synthesized either directly from a metal oxide or by double decomposition where a metal acetate is first reacted with ammonium neodecanoate

formed from neodecanoate acid followed by removal of the ammonium acetate from the solid by washing it in water. The metallorganic precursor is formed by dissolving the solid in a suitable solvent such as xylene, toluene, or tetrahydrofuran (THF). Metallorganics dissolved in solvents mix at the atomic level and thus are true solutions and thus are typically very stable and have long shelf lives.

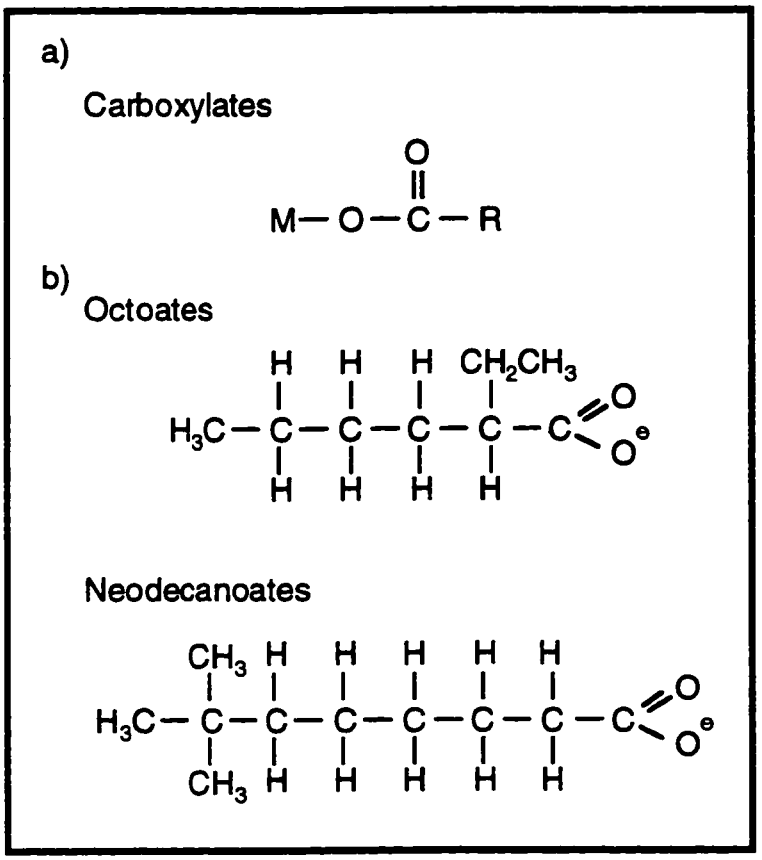

Fig. A.1: (a) Typical Carboxylate and (b) Two typical R groups: Octoates and Neodecanoates.

A.2: Deposition Techniques

This technique has been successfully used to a wide variety of materials on different substrates. These include films such as $YBa_2Cu_3O_7$, Pt, Au, Ag, Pd, $PbTiO_3$, ITO, $BaTiO_3$ and $SrTiO_3$ films on substrates such as Si, Pt coated Si, Pt, and platinum caoted yttiria. The variety in materials that can be deposited using MOD is matched by the variety in the deposition methods. The most common deposition technique is by dispensing the

metallorganic liquid from a standard resist coater. Other deposition techniques that are less frequently used include screen printing, spray and dip coating[2].

In MOD, a suitable metallorganic precursor is dispensed onto a substrate which is then spun at a few thousand revolutions per minute and in the process forming a uniform organic film. This is followed by pyrolyzing the soft film in air, oxygen, nitrogen or any other suitable atmosphere to convert the organic films into their constituent elements, oxides or other compounds depending on the exact composition of the metallorganic precursor and the type of annealing atmosphere used. In the case of oxides, it is common to anneal the organic films first at low temperature (500°C) in air for few minutes to convert the metallorganic film into its oxide. These films are usually polycrystalline and the grain sizes are very small. Therefore, it is customary to follow the low temperature annealing by high temperature annealing (800-900°C) in oxygen for longer periods to enhance grain growth and remove excess carbon in the films. Depending on the type of substrate used, the high temperature annealing step is also used to promote preferred epitaxial grain growth.

Films prepared by MOD react to energetic beams of focused particles or light prior to annealing in a manner similar to photoresists used in IC technology. Selective exposure of the films renders only the exposed metallorganic insoluble in the solvent, thus allowing the unexposed areas to be developed away in the starting solvent. This property makes these films suitable for fabricating fine lines and various geometries used in interconnects and sensors.

Metallorganic decomposition is a simple, inexpensive means of film deposition which is compatible with very-large-scale integrated circuit (VLSI) technology and has been used for depositing device-quality films for sensors and other novel devices. However, the importance of this technique lies in the fact that it is very beneficial in studying substrate interactions and the effects of temperature on grain growth.

REFERENCES

Chapter 1

1. M. E. Lines and A. M. Glass, *Principles and Applications of Ferroelectrics and Related Materials* (Clarendon, Oxford, 1977).

2. M. Deri, *Ferroelectric Ceramics* (Gordon and Breach , New York, 1969).

3. F. Jona and G. Shirane, *Ferroelectric Crystals* (Pergamon, New York, 1962).

4. C. B. Sawyer and C. H. Tower, Phys. Rev. **35**, 269 (1930).

5. A. von Hippel, R. G. Breckenridge, F. G. Chesley, and L. Tisza, Ind. Eng. Chem. **38**, 1097 (1946).

6. B. Wull, and I. M. Goldman., Compt. rend. Acad. Sci. U.R.S.S. **46**, 139 (1945).

7. J. Valasek, Phys. Rev. 17, **475** (1921).

8. J. P. Remika, J. Am. Chem. Soc. **76**, 940 (1954).

9. T. Mitsui, I. Tatsuzaki, and E. Nakamura, *An Introduction to the Physics of Ferroelectrics* (Gordon and Breach , New York, 1976).

10. G. A. Smolenskii, Doklady Akad. Nauk S.S.S.R. **70**, 405 (1950).

11. G. A. Smolenskii, Zhur. Tekh. Fiz. **20**, 137 (1950).

12. J. K. Hulm, Proc. Phys. Soc. **63**, 1184 (1950).

13. A. Kain, C. Pettiette-Hall, K. Daly, A. Lee, R. Hu and J. Burch, IEEE Transactions on Applied Superconductivity, **3** (1993) 1421.

14. I. Kobayashi, Y. Wakao and M. Okada, Jpn. J. Appl. Phys., **33** (1994) 4680.

15. J. Nowotny, and M. Rekas, Key Eng. Mat. **66 & 67**, 45 (1992).

16. A. F. Devonshire, Phil. Mag. **40**, 1040 (1949).

17. A. F. Devonshire, Phil. Mag. **42**, 1065 (1951).

18. A. F. Devonshire, Adv. Phys. **3**, 85 (1954).

19. J. C. Slater, Phys. Rev. **78**, 748 (1950).

20. J. C. Slater, *Ferroelectricity*, edited by E. F. Weller (Elsevier, New York, 1967).

Chapter 2

1. J. V. Mantese, N. W. Schubring, A. L. Micheli, and A. B. Catalan, Appl. Phys. Lett. **67**, 721 (1995).

2. V. L. Gurevich, Sov. Phys. Solid State **23** (8), 1377 (1981).

3. F. Jona and G. Shirane, *Ferroelectric Crystals* (Pergamon, New York, 1962)

4. B. A. Strukov, A. V. Davtyan, and E. L. Sorkin, Sov. Phys. Solid State **25** (4), 627 (1983).

5. B. A. Strukov, A. V. Davtyan, and E. L. Sorkin, Sov. Phys. Solid State **25** (4), 627 (1983).

6. H. J. Sajosch, Int. J. Mod. Phys. (B) **4**, 501 (1990).

7. D. R. Tilley, Sol. Sta. Comm. **65**, 657 (1988).

8. Shaoping Li, J. A. Eastman, R. E. Newnham, and L. E. Cross, Phys. Rev. (B) **18**, 1 (1997).

9. D. R. Tilley, and B. Zeks, Sol. Sta. Comm. **49**, 823 (1984).

10. C. L. Wang and S.R.P. Smith, Sol. Sta. Comm. **99**, 559 (1996).

11. B. S. Kwak, A. Erbil, B. J. Wilkens, J.D. Budai, M.F. Chisholm, and L.A. Boatner, Phys. Rev. Lett. **68**, 3733 (1992).

12. B. S. Kwak, A. Erbil, J. D. Budai, M. F. Chisholm, L. A. Boatner, and B. J. Wilkens, Phys. Rev. B **49**, 14865 (1994).

13. K. Kajiyoshi, N. Ishizawa, and M. Yoshimura, Jap. J. Appl. Phys. **30**, 120 (1991).

14. N. W. Schurbring, J. V. Mantese, A. L. Micheli, A. B. Catalan, and R. J. Lopez, Phys. Rev. Lett. **68**, 1778 (1992).

Chapter 3

1. L. C. Sengupta, E. Ngo, M. E. O'Day, and R. Lancto, Proceeding of the 1994 IEEE 13th International Symposium on Applications of Ferroelectrics, 622 (1995)

2. E. Wiener-Avnear, Appl. Phys. Lett. **65**, 1784 (1994).

3. H. Kawano, K. Morii, and Y. Nakayama, J. Appl. Phys. **73**, 5141 (1993).

4. A. B. Catalan, J. V. Mantese, A. L. Micheli, N. W. Schubring, and R. Poisson, J. Appl. Phys. **76**, 2541 (1994).

5. D. Tahan, A. Safari, and L. C. Klein, Proceeding of the 1994 IEEE 13th International Symposium on Applications of Ferroelectrics, 427 (1995).

6. D. Roy, and S. B. Krupanidhi, Appl. Phys. Lett. **62**, 1056 (1993).

7. N. W. Schubring, J. V. Mantese, A. L. Micheli, A. B. Catalan, and R. J. Lopez, Phys. Rev. Lett. **68**, 1778 (1992).

8. K. Abe, and S. Komatsu, J. Appl. Phys. **77**, 6461 (1995).

9. J. V. Mantese, N. W. Schubring, A. L. Micheli, and A. B. Catalan, Appl. Phys. Lett. **67**, 721 (1995).

10. J. V. Mantese, A. L. Micheli, A. H. Hamdi, and R. W. Vest, MRS Bull., **Oct.**, 48 (1989).

11. B. D. Cullity, "Elements of X-ray Diffraction", 2nd ed. (Reading, MA., Addison-Wesley, 1978).

12. Swanson, and Fuyat, NBC Circular 539, vol. III (1953).

13. A. G. Chynoweth, Phys. Rev. **102**, 705 (1956).

14. Y. Xu, C. G. Chen, R. Xu, and J. D. Mackenzie, J. Appl. Phys. **67**, 2985 (1990).

15. J. J. Xu, A. S. Shaikh, and R. W. Vest, IEEE Trans. Ultrason., Ferroelectr., Freq Control **36**, 307 (1989).

16 A. S. Shaikh, R. W. Vest, and G. M. Vest, IEEE Trans. Ultrason., Ferroelectr., Freq Control **36**, 407 (1989).

17. Y. Miyasaka, and S. Matsubara, Proceeding of the 1990 IEEE 7th International Symposium on Applications of Ferroelectrics, 121 (1990).

18. J. Nowotny, and M. Rekas, Key Eng. Mat. **66** & **67**, 45 (1992).

19. G. Arlt, D. Hennings, and G. de With, J. Appl. Phys. **58**, 1619 (1985).

20. B. Jaffe, and W. R. Cook, "Piezoelectric Ceramics" (Academic, London, 1971).

21. A. B. Catalan, J. V. Mantese, A. L. Micheli, N. W. Schubring, and C. A. Wong, J. Am. Ceram. Soc. **75**, 3007 (1992).

Chapter 4

1. B. S. Kwak, A. Erbil, B. J. Wilkens, J. D. Budai, M. F. Chisholm, and L. A. Boatner, Phys. Rev. Lett. **68**, 3733 (1992).

2. B. S. Kwak, A. Erbil, J. D. Budai, M. F. Chisholm, L. A. Boatner, and B. J. Wilkens, Phys. Rev. B **49**, 14865 (1994).

3. N. W. Schurbring, J. V. Mantese, A. L. Micheli, A. B. Catalan, and R. J. Lopez, Phys. Rev. Lett. **68**, 1778 (1992).

4. J. V. Mantese, N. W. Schurbring, A. L. Micheli, and A. B. Catalan, Appl. Phys. Lett. **67**, 721 (1995).

5. J. C. Slater, *Ferroelectricity* (Elsevier, New York, 1967), Ed. E.F. Weller, pp. 1-8.

6. J. C. Slater, *Insulators, Semiconductors and Metals* (McGraw-Hill, New York, 1967), pp. 198-203.

7. J. C. Slater, *Insulators, Semiconductors and Metals* (McGraw-Hill, New York, 1967), pp. 95-100.

8. J. C. Slater, Phys. Rev. **78**, 748 (1950).

9. F. Jona and G. Shirane, *Ferroelectric Crystals* (The Macmillan Co., New York, 1962), pp. 216-279.

10. S. Triebwasser, Phys. Rev. **114**, 63 (1959).

11. V. L. Gurevich, Sov. Phys. Solid State **23** (8), 1377 (1981).

12. B. A. Strukov, A. V. Davtyan, and E. L. Sorkin, Sov. Phys. Solid State **25** (4), 627 (1983).

13. B. A. Strukov, A. V. Davtyan, and E. L. Sorkin, Sov. Phys. Solid State **25** (4), 627 (1983).

14. H. J. Sajosch, Int. J. Mod. Phys. (B) **4**, 501 (1990).

15. M. S. Mohammed, R. Naik, J. V. Mantese, N. W. Schubring, A. L. Micheli, and A. B. Catalan, J. Mater. Res., **11**, 2588 (1996).

16. A. L. Micheli, J. V. Mantese, and N. W. Schubring, Int. Ferr. **12**, 1 (1996).

17. C. B. Sawyer and C. H. Tower, Phys. Rev. **35**, 269 (1930).

18. R. L. Moreira and R. P. S. M. Lobo, Jour. Phys. Soc. Jap. **61**, 1992 (1992).

19. N. Singh, A. P. Singh, C. D. Prasa, and D. Pandey, Jour. Phys. Cond. Mat. **8**, 7813 (1996).

20. R. P. S. M. Lobo, R. L. Moreira, and N. D. S. Mohallem, Ferr. **133**, 169 (1992).

21. T. R. Halemane, M. J. Haun, L. E. Cross, and R. E. Newnham, Ferr. **62**, 149 (1985).

22. W. Kinase and K. Mori, Ferr. **29**, 235 (1980).

Chapter 5

1. C. Lucas, *Sensors and Actuators A*, **25-27** (1991).

2. R. W. Whatmore, P. C. Osbond, and N. M. Shorroks, *Ferroelectrics*, **76**, 351 (1987).

3. P. W. Kruse, *Proc.11th Int. Symp. Appl. Ferroelectrics*, IEEE, 643 (1995).

4. C. Hanson, H. Beratan, *Proc.11th Int. Symp. Appl. Ferroelectrics*, IEEE, 657 (1995).

5. N. W. Schubring, J. V. Mantese, A. L. Micheli, A. B. Catalan, and R. J. Lopez, *Phys. Rev. Lett.* **68**, 1778 (1992).

6. M. S. Mohammed, R. Naik, J. V. Mantese, N. W. Schubring, A. L. Micheli, and A. B. Catalan, *J. Mater. Res.*, **11**, 2588 (1996).

7. J. V. Mantese, N. W. Schubring, A. L. Micheli, and A. B. Catalan, *Appl. Phys. Lett.*, **67**, 74 (1995).

8. B. Cole, R. Horning, B. Johnson, K. Nguyen, P. W. Kruse, and M. C. Foote, *Proc.11th Int. Symp. Appl. Ferroelectrics*, IEEE, 653 (1995).

9. J. V. Mantese, N. W. Schubring, A. L. Micheli, A. B. Catalan, M. S. Mohammed, R. Naik, and G. W. Auner, Appl. Phys. Lett., **71**, 2074 (1997).

10. B. M. Kulwicki, A. Amin, H. Beratan, and C. Hanson, *Proc.8th Int. Symp. Appl. Ferroelectrics*, IEEE, 1 (1992).

Appendix A:

1. J. V. Mantese, A. L. Micheli, A. H. Hamdi, and R. W. Vest, MRS Bull., **Oct.**, 48 (1989).

2. A. M. Mance, J. V. Mantese, and A. L. Micheli, General Motors Research and Development Center internal report (R&D 8723). To be publishd in Monogarph, a Springer Verlag publication.

ABSTRACT

GRADED FERROELECTRIC DEVICES:
THE DIELECTRIC ANALOGUES OF SEMICONDUCTOR DIODE JUNCTIONS

by

MAJED S. MOHAMMED

May 1998

Advisor: Dr. Gregory W. Auner

Major: Electrical Engineering (Solid State Devices)

Degree: Doctor of Philosophy

This study demonstrates that a new pyroelectric device can be created from ferroelectrics with gradient in composition, and that the field dependence of the observed hysteresis offset is as predicted from theory.

Homogeneous thin films of $Ba_xSr_{1-x}TiO_3$ (x=0.7, 0.8, 0.9, and 1.0) were prepared by metallorganic decomposition (MOD). The relative permittivity, dissipation, polarization, resistivity, and grain size were studied as a function of composition and temperature. Ferroelectric hysterisis loops were observed for all values of x and were found to be independent of measurement temperature though strongly dependent upon grain size.

Ferroelectric BST thin films with compositional gradients normal to the growth surface have been formed by successive deposition and annealing of films having step-variable Ba to Sr ratios. These films, graded ferroelectric devices or GFD's, are the

dielectric equivalent of the semiconductor p-n and n-p junctions. Unlike semiconductor diode junctions which have a built-in potential arising from the diffusion of free charge across the junction, the intrinsic potential in graded ferroelectric devices is due to a gradient in bound charge. In their simplest forms, graded ferroelectric devices give rise to a totally new, but controllable hysteresis phenomenon that is not observed in homogenous ferroelectric materials.

Slater's empirical model for ferroelectric materials has been also extended to describe the graded ferroelectric devices. This model accounts for several aspects of these structures including: the broadness of the permittivity plots with temperature, the formation of a spontaneous potential upon oscillatory field excitation, offsets in the hysteresis graphs along the displacement axis with directions which are gradient dependent, and the electric field dependence of that offset.

The graded ferroelectric devices, as formed by MOD, show very low conventional pyroelectric coefficient. However, the effective pyroelectric coefficients obtained from these active devices were much greater, reaching a maximum of 0.06 $\mu C/cm^2$-°C, compared to conventional value of 0.045 $\mu C/cm^2$-°C for homogeneous BST films. This study demonstrates that the method used to fabricate the GFD's is inadequate to produce the desired sensitivity. Suggestions for ways to increase the sensitivity of the GFD's are given.

AUTOBIOGRAPHICAL STATEMENT

I was born in May 17, 1965 in Kuwait City, Kuwait. I am the youngest of five brothers. Both of my parents were born and raised in Burqa, a small village 20 miles north of Nablus, the largest city in the West Bank, Palestine. I finished High school in 1983. Immediately after graduation I left Kuwait to Jordan were I studied physics and computer science. I received my Bachelor of Science degree in June 1987 from Yarmouk University, Irbid.

I obtained my Master of Science degree in August 1991 from King Fahd University of Petroleum and Minerals, Dhahran, Saudi Arabia. Afterwards, I worked as a lecturer in the physics department at KFUPM for 3 years. I joined the doctorate program at Wayne State University in 1994. As part of my doctorate dissertation work, I spent four years as a member of a research team at General Motors Technical Center engaged in developing a new and economical infrared night vision system based on graded ferroelectric materials.

I have the following publications:

1. "Microstructure and Ferroelectric Properties of Fine-Grained $Ba_xSr_{1-x}TiO_3$ Thin Films Prepared by Metallorganic Decomposition," M. Mohammed, R. Naik, J. Mantese, N. Schubring, A. Micheli, and A. Catalan., *J. Mater. Res.* **11**, 2588 (1996).
2. "Slater Model Applied to Polarization Graded Ferroelectrics," J. Mantese, N. Schubring, A. Micheli, A. Catalan., M. Mohammed, R. Naik, and G. Auner, *Appl. Phys. Lett.* **71**, 2047 (1997).

I am married to a most wonderful person. Dima and I currently live in Windsor, Canada.